VALORIZATION OF ASHE JUNIPER WASTE INTO HIGH VALUE-ADDED PRODUCTS: FUNCTIONALIZED BIOCHAR AND HIGH VALUE CHEMICALS

A Dissertation

by

JULIUS LEE CHOI

Submitted to the Office of Graduate and Professional Studies of
Texas A&M University
in partial fulfillment of the requirements for the degree of

DOCTOR OF PHILOSOPHY

Chair of Committee,	Sergio C. Capareda
Committee Members,	Gary Riskowski
	Sandun Fernando
	Mahmoud El-Halwagi
Head of Department,	Stephen W. Searcy

December 2017

Major Subject: Biological and Agricultural Engineering

ABSTRACT

Current biomass waste management such as landfills and combustion negatively affects the environment and public health. It is recognized that the production of biomass waste is unavoidable. Globally, 150 to 170 billion tons of biomass waste is annually available. For example, in central Texas, large amounts of Ashe Juniper waste is produced by the current management practices (hydraulic shear or bulldozer) to control population. However, biomass waste is expected as the only potential renewable carbon source alternative to petroleum-based products. Therefore, the development of the method to utilize biomass waste as carbon resource for the production of value-added products is highly required.

In this dissertation, the methods for controlling biochar properties, and producing surface functionalized biochar and high value-added chemicals are developed. The method to control biochar properties is based on the concept of vacuum pyrolysis. By investigation of effects of vacuum pressure and temperature on the physicochemical properties of biochar, we confirmed that this method enabled us to produce biochar having potential applications as an adsorbent, a catalyst support, and a carbon sequestration agent. The method to produce functionalized biochar with high adsorption capacity for wastewater treatment was developed based on sulfuric acid treatment. The concentration of sulfuric acid was an important factor to control the adsorption capacity. The change of adsorption capacity was correlated to physicochemical properties such as surface area and surface functional groups. The developed functionalized biochar showed approximately

200 times improved adsorption capacity for dye chemicals compared to raw biochar. The influence of adsorption process parameter was conducted. Also, the biochar showed potential as a promising separator of certain dye chemicals in a multicomponent system. The method to obtain a high selectivity of Levoglucosenone (LGO), Furfural (FF), and levoglucosan is developed using catalytic pyrolysis and microwave-assisted pretreatment. LGO was only produced after treatment with $CuSO_4$ and $ZnSO_4$, which was attributed to dehydration of levoglucosan. Metal salt type and concentration affected the selectivity of LGO and FF by catalytic vacuum pyrolysis. Microwave solvothermal treatment affected pyrolysis characteristics and increased the selectivity of levoglucosan by approximately nine times.

DEDICATION

To my future wife Yuri Kim and wonderful parent and sister, who have supported my journey…

ACKNOWLEDGEMENTS

I would like to thank the committee chair, Dr. Capareda, and committee members, Dr. Riskowski, Dr. Fernando, and Dr. El-halwagi for their guidance and support throughout the course of this research.

Thanks also go to my current and previous collegues, friends and colleagues, department faculties and staff for making my time a great experience.

Finally, special thanks to my mother, father, and sister for their unconditional support and love, and to my lovely girlfriend for her patience and love.

CONTRIBUTORS AND FUNDING SOURCES

This work was supervised by a dissertation committee consisting of Professor Sergio C. Capareda (advisor), Gary Riskowski, and Sandun Fernando of the Department of Biological and Agricultural Engineering and Professor Mahmoud El-Halwagi of the Department of Chemical Engineering.

The analyses depicted in Chapter 2 were conducted in part by Hyungseok Nam in Auburn Universiy and Seaborn Carter of the Department of Biological and Agricultural Engineering and were published in 2017.

All other work conducted for the dissertation was completed by the student independently.

Graduate study was supported by the facilities, the scientific and financial assistance of the Bio Energy Testing and Analysis Laboratory and AgriLife Research at Texas A&M University.

NOMENCLATURE

ANOVA	Analysis of Variance
ASTM	American Society for Testing and Materials
BAC	Benzalkonium Chloride
BET	Brunauer-Emmett-Teller
BETA Lab	Bio-Energy Testing and Analysis Laboratory
FC	Fixed Carbon
FF	Furfural
FTIR	Fourier-Transform Infrared Spectroscopy
GC	Gas Chromatography
LGO	Levoglucosenone
MS	Mass spectroscopy
PID	Proportional-integral-derivative
TGA	Thermogravimetric Analysis
DTG	Derivative Thermogravimetric Analysis
UV	Ultra-Violet
VM	Volatile Matter

TABLE OF CONTENTS

Page

LIST OF FIGURES

Page

LIST OF TABLES

CHAPTER I

INTRODUCTION

Raw biomass waste is composed of forestry and agricultural resources, industrial process residues, and municipal-solid and urban-wood waste, which are abundant and readily available[1]. Globally, 150 to 170 billion tons are available annually[2]. In the agricultural industry, massive amounts of biomass waste are produced in harvesting, processing, and using agricultural products including food[3]. For example, 1394.49 million tons of agricultural waste such as wheat straw, rice straw, corn straw and sugarcane bagasse was available in 2012[2, 4]. Furthermore, the volume of food waste including municipal-solid waste is estimated at 1.76 billion tons[5]. In the US, annually, 47 million dry tons of logging residue is available according to the Billion-Ton Update in August 2011 reports[6]. Currently, most of the biomass waste is managed by landfill and combustion which have a negative effect on the environment and public health[3, 7]. However, it is recognized that the production of biomass waste is not avoidable[3]. Therefore, the development of ways to create value from this unavoidable waste is highly required.

Biomass waste is the only renewable carbon resource alternative to petroleum-based products and has the great potential for producing energy (e.g., bio-energy)[2, 6] which is one of the renewable energy sources, functional materials (e.g., biochar and nanocellulose)[8, 9] ,and high-value-added chemicals (e.g., levoglucosenone and acetol)[2]. In

past years, biomass valorization has attracted great attention and been intensively investigated[2, 6].

Pyrolysis, which is the heating of organic material such as biomass in the absence of oxygen, is one of the valorization methods[10]. By the pyrolysis process, biomass can be converted to biochar, syngas, and bio-oil[6]. These products can be used to create fuels for heat, power, and transportation alternatives to conventional fuels[6]. However, these products have other valuable potential applications other than alternative fuels.

Biochar is a carbon-rich and porous, solid material. Recently, biochar has attracted increasing attention as a carbon sequestration agent with the ability to mitigate greenhouse gas emissions[11, 12]. It also has applications as a soil amendment capable of improving soil health. Also, biochar has demonstrated potential as a contaminant adsorbent, carbon catalyst, and catalyst support[8, 9]. Furthermore, biochar can be used as a platform for the synthesis of various functionalized carbon materials[8]. These applications are attributed to the properties of biochar such as high surface area, porosity, abundant surface functional groups, (oxygen contained functional groups) and stability in acid or base conditions[8]. Therefore, the development of the method to tune the physicochemical properties of biochar is crucial for expanding and controlling its functionality.

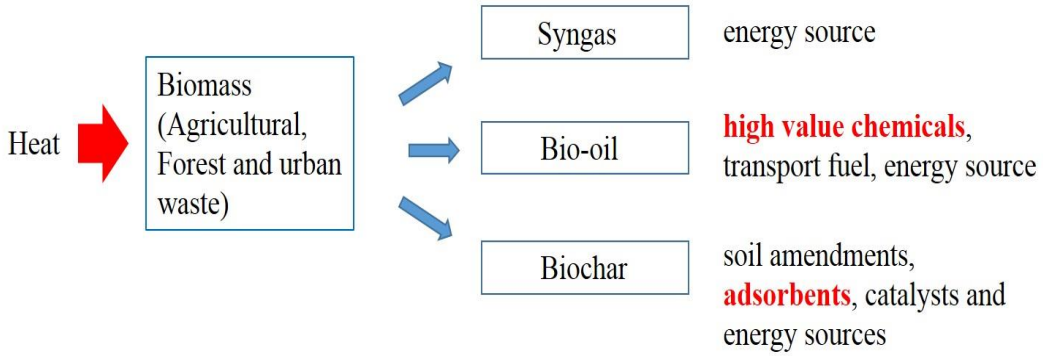

Figure 1. Pyrolysis process for biomass conversion to valuable products

Peak temperature and pressure have critical effects on the yields, physical, and chemical properties of biochar[8, 11]. According to several studies, increasing peak temperature tends to lower biochar yields[8, 11, 13]. Moreover, the fixed-carbon content increases as peak temperature increases[14-16]. The peak temperature also affects two important textural properties (surface area and porosity)[8, 11, 14]. Surface area tends to increase as peak temperature increases. The elemental composition also depends on the peak temperature[8, 17]. Further investigation of peak temperature revealed that the H/C and O/C ratios that are related to the aromaticity of biochar decreased with increasing peak temperature[16, 18, 19]. Also, O/C and (O+N)/C are parameters related to polarity and surface functional groups on biochar[20]. Higher O/C and (O+N)/C means more oxygen-contained functional groups in biochar.

Pressure is another critical process parameter for the pyrolysis process that results in changes for biochar production. Biochar yields tend to increase with pyrolysis pressure probably due to an increased vapor residence time in the biomass particle which leads to

a secondary charring reaction[15]. The contents of fixed carbon in biochar also increase with higher pyrolysis pressure[15, 21, 22]. Pressure conditions also influence the textural properties of the biochar produced. Centin et al. confirmed that a slight decrease of the total surface area was caused by increasing pressure[23]. Also, a dramatic decrease of BET surface area of biochar with increasing pressure was observed due to a clogging of the pores by tar deposits[24]. These results mean that high pressure inhibits the production of biochar with high surface area and good porosity. However, there is no report regarding the influence of vacuum pressure on the textural properties of biochar. Vacuum pressure is expected to introduce high surface area and well-developed porosity to biochar because of decreased vapor residence time in biomass during pyrolysis. In this study, the effect of peak temperature and vacuum pressure on the properties of biochar was investigated to develop the method to control the potential application of biochar.

Biochar has an optimistic potential for use as a low-cost adsorbent for the removal of contaminants. Currently, many contaminants (metal ions, organics, and anions) in wastewater have been removed by chemical and biological methods[17, 25]. Adsorption is expected as the most efficient method to remove contaminants[17, 25]. Especially activated carbon, which is normally derived from coals, is thought of as a universal adsorbent for removing contaminants. However, the production cost of activated carbon limits the practical application. On the other hand, biochar requires less investment compared to activated carbon[26]. Biochar also exhibits potential for water purification by absorbing hydrocarbons, other organics, and some inorganic metal ions[17, 25]. Therefore, biochar is expected as a low-cost adsorbent as a water treatment alternative to activated carbon.

However, there are some hurdles to overcome for the commercialization of biochar as an adsorbent owing to relatively low adsorption capacity and removal efficiency[25]. For example, biochar showed a lower adsorption capacity for dye chemicals in wastewater than other conventional adsorbents. Biochar should be engineered to get higher adsorption capacity or removal efficiency on contaminants for the commercialization[25].

The disposal of dye chemicals, used in textile dyeing, paper printing, and other industries, can eventually cause serious damage to the environment due to their toxic, mutagenic, or carcinogenic properties[27]. The adsorption process has been found to be an effective and attractive process for removal of dye contaminants. Even though biochar has shown promising results regarding the removal of dye materials, the biochar showed low adsorption capacities compared to conventional adsorbents[25], and these investigations were conducted at a concentration lower than 200 mg/L[17, 25, 27]. For practical applications, the adsorption capacity of biochar should be reliable even under investigation at a concentration higher than 300 mg/L, which is practically the final dye concentration in effluents[27]. Therefore, for the practical application of biochar in wastewater treatment, biochar with high adsorption capacities even at high dye concentration, should be produced. Moreover, most of the biochar adsorption studies were conducted in a single component system. For the practical application of biochar adsorption process, an adsorption study in a multicomponent system is required. In this study, the surface of biochar produced from biomass waste was functionalized using acid-treatment to get higher adsorption capacity or removal efficiency on dye chemicals in the multicomponent system.

Bio-oil is composed of hundreds of chemicals. Bio-oil includes some high-value-added chemicals (e.g. levoglucosenone, levoglucosan and furfural)[2, 28]. For example, levoglucosenone can be used as a building block[29, 30] for the synthesis of pharmaceuticals such as (+)-chloriolide (antibiotic) and ras proteins activation inhibitors (anticancer drug), 1,6-hexanediol widely used for the production of polyester, polyamide and polyurethane, and 5-hydroxymethyldihydrofuranone (5-HMF) for pharmaceuticals, fuels and nucleic acids. Therefore, bio-oil is an excellent raw source to obtain specific value-added chemicals. High value-added chemicals can be recovered from bio-oil by separation processes such as distillation[31]. However, the recovery of the high value-added chemicals from bio-oils is still technically challenging and less economical because of the complexity of composition and low concentration of all components in bio-oils. Therefore, the production rate and selectivity of certain required chemicals should be improved for commercialization. Selective pyrolysis is the only way to produce high-value chemicals with high production rates and selectivity from biomass.

Levoglucosenone (LGO) is rarely produced from raw biomass by pyrolysis[28]. To increase the production rate and selectivity of LGO, several catalytic pyrolysis tests were conducted. Dobele et al. conducted catalytic pyrolysis with phosphoric acid-impregnated cellulose and biomass, which resulted in the maximum selectivity of 30%[32, 33]. Dobele et al. also investigated the effect of Fe^{3+} on the yield of LGO, of which maximum yield was 25.7%, derived from cellulose[34]. Branca et al. investigated acid-catalyzed pyrolysis of concorbs with the 4.6% yield of LGO[35]. Solid acids such as sulfated ZrO2, sulfated TiO2, and sulfated TiO2/Fe2O3 were explored to improve the yield of LGO based on cellulose

to 7.25%[36], 5.69%[36] and 15.43%[37], respectively. Xin et al. reported up to 82.6% of LGO selectivity from cellulose impregnated with phosphoric acid by an evaporation method[28]. Xin et al. also concluded that sulfates could increase the LGO yield significantly[28]. However, these studies focused on the pyrolysis of cellulose. There is no report regarding the production of levoglucosenone from raw biomass waste. Furthermore, the effect of kind and concentration of cations and pretreatment of biomass waste on the selectivity of levoglucosenone is not investigated. In this study, we tested the influences of the process parameter, catalyst, and pretreatment on the selectivity of the high-value-added chemicals produced by vacuum pyrolysis.

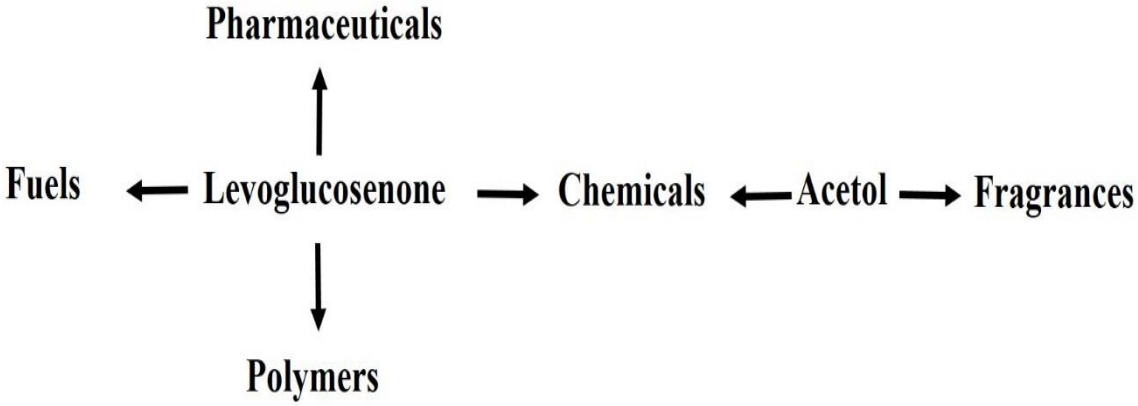

Figure 2. Potential use of Levoglucosenone

Ashe juniper (*Juniperus ashei Buchholz*) is a native species covering over 8 million acres of Texas rangelands[38]. The rapid spread of Ashe juniper across Texas has altered the

production, composition, and structure of rangeland plant communities[39]. Furthermore, the intrusion of Ashe juniper in Texas rangelands may influence the hydrological landscape of government protected lands[39]. For example, it has been reported that approximately 40 to 43% of rainfall is intercepted by Ashe juniper[38]. Current best management practices for removing Ashe juniper over widespread areas include the use of hydraulic shears or bulldozers followed by burning, which is not economically feasible[40]. Ashe juniper contains some essential oils that are commercially valuable in the flavor and fragrance industries[41, 42]. Therefore, the extraction of essential oils is one way to valorize Ashe juniper wastes. However, there are still a lot of Ashe juniper wastes left after the extraction of essential oils. Therefore, the development of the new way to valorize Ashe Juniper waste is crucial to expanding the utility of Ashe Juniper waste. In this thesis, Ashe Juniper waste was selected as a model biomass waste.

The overall goal of this doctoral study is to convert Ashe Juniper waste into high value-added products using the pyrolysis process. Specifically, this doctoral study was dedicated to 1) The modification of the physicochemical properties of biochar, 2) The adsorption study of functionalized biochar for a contaminant removal and 3) Selective production of high-value-added chemicals: Levoglucosenone, Levoglucosan, and furfural.

CHAPTER II

TUNING THE PHYSICOCHEMICAL PROPERTIES OF BIOCHAR DERIVED FROM ASHE JUNIPER BY VACUUM PRESSURE AND TEMPERATURE*

2.1 Introduction

Biochar, a carbon-rich and porous solid material, has recently attracted increasing attention as a carbon sequestration agent with the ability to mitigate greenhouse gas emission[9]. It can also be used as a soil amendment capable of improving soil health and demonstrated potential as a contaminant adsorbent, carbon catalyst and catalyst support[8, 9]. The biochar's diverse potential is attributed to its physicochemical properties-high surface area, porosity, surface functionality and the degree of carbonization[8]. Therefore, the development of the method to tune the desired properties of biochar would be helpful for use of biochar in various applications.

Biochar is normally produced through the slow pyrolysis of biomass. Peak temperature and pressure have critical effects on the yields, physical and chemical properties of biochar[8, 11]. Increasing peak temperature tends to lower biochar yields[8, 11, 13] while increasing the fixed-carbon content[14-16]. The peak temperature also affects two important textural properties (surface area and porosity) with surface area increasing as peak temperature increases[8, 11, 14]. The elemental composition also depends on the peak

* Modified and reprinted with permission from "Tuning the physicochemical properties of biochar derived from Ashe juniper by vacuum pressure and temperature" by Julius Choi, Hyungseok Nam, Seaborn Carter, and Sergio C. Capareda, Journal of Environmental Chemical Engineering 5 (4), 3649-3655, Copyright 2017, Elsevier

temperature[8, 17]. Further investigation of peak temperature revealed that increasing peak temperature lowered the H/C and O/C ratios, which are related to the aromaticity of biochar[16, 18, 19]. The degree of aromaticity may be indirectly proportional to the degree of chemical recalcitrance in soils[15, 43]. In addition, O/C and (O+N)/C are parameters related to polarity and surface functional groups on biochar[20]. Higher O/C and (O+N)/C means more oxygen-contained functional groups in biochar. The surface functionality acts as an active site for nutrient retention of biochar in soil and the functionalization of biochar[8].

As pressure increases, biochar yield increases most likely due to an increased vapor residence time in the biomass particle which leads to a secondary charring reaction [15]. The contents of fixed carbon in biochar also increase with higher pyrolysis pressure[15, 22]. Pressure conditions also influence the textural properties of the biochar produced. Increasing pressure led to a decrease of BET surface area of biochar due to a clogging of the pores by tar deposits[11]. High pressure thus inhibits the production of biochar with high surface area and good porosity. Well-developed biochar characteristics are required for the application of biochar as soil amendments, adsorbents or catalyst support applications.

To improve textural properties of biochar, the secondary charring reactions, which are the condensation of volatiles and solid-vapor phase reactions, need to be minimized. The secondary reaction can be prevented by removing volatiles quickly from biomass. Vacuum pyrolysis can be one of the best options to minimize the secondary reaction due to its special advantage of minimum vapor residence time during pyrolysis[43]. Several studies have shown that activated carbon with a high surface area and porosity can be developed under vacuum pressure[44]. Not only textural properties but also the

aforementioned chemical properties should be controlled for the specific application of biochar. The chemical properties can be changed by varying the pyrolysis temperature. However, the effect of vacuum pressure on aforesaid chemical properties of biochar is rarely found in the literature[45]. Furthermore, synergistic effects of vacuum pressure and temperature on textural and chemical properties of biochar are rarely investigated[45].

Here, Ashe juniper was selected as a biomass waste model for the investigation. Ashe juniper, a native species covering over 8 million acres of Texas rangelands[38], has rapidly spread across Texas altering the production, composition, and structure of rangeland plant communities[39]. The intrusion of Ashe juniper on Texas rangeland may influence the hydrological landscape of government-protected lands[39]. For example, it has been reported that approximately 40 to 43% of rainfall is intercepted by Ashe juniper[38]. Current best management practices for removing Ashe juniper over widespread areas include the use of hydraulic shears or a bulldozer, followed by burning[40], which are not economically feasible. One way to improve the economic value of Ashe juniper management is to extract essential oils, which are commercially valuable in the flavor and fragrance industries, from Ashe juniper[41]. Another method could be producing fences from Ashe Juniper[41]. However, a large quantity of Ashe juniper wastes might be left even after both processes. Also, Ashe juniper might be a promising resource to produce high-quality carbonaceous materials due to relatively high carbon contents determined in the current study. Therefore, the conversion of Ashe juniper waste into biochar through pyrolysis will be one valorization method.

To the best of our knowledge, there is no report focused on vacuum pyrolysis of Ashe juniper as a feedstock for biochar production. The main objective of this project is to evaluate the effects of temperature and vacuum pressure on the properties of biochar derived from Ashe juniper biomass. The specific objectives are as follows:

a. To characterize the combined effect of temperature and vacuum pressure on the biochar properties (elemental composition, degree of carbonization, proximate analysis, surface functionality, and textile structures),
b. To determine the potential application of tuned biochar based on the properties, and
c. To evaluate the removal capacity of biochar as an adsorbent on a target chemical.

2.2 Materials and methods

2.2.1 Feed material

Ashe Juniper was obtained by thinning from Hills Country (TX, USA). Ashe juniper was crushed in a Wiley mill using a 2 mm screen and the crushed samples were stored in a zip-lock bag at room temperatture. The samples were dried for 2 hours in a convection oven at 105°C before pyrolysis. The volatility, fixed carbon and ash contents were determined following ASTM E870-82[21]. The elemental composition was determined with an ultimate analyzer (Vario MICRO elemental analyzer).

2.2.2 Vacuum pyrolysis for the production of oils and biochar

Ashe juniper was pyrolyzed in a vacuum pyrolysis machine as shown in Figure 3. For each experiment, 10 g of the raw biomass was placed in a glass flask (Chemglass), before inserting into an electrical furnace. The main flask was connected to a condenser for collection of the heavy fraction (Fraction 1) located before a cold trap (-196°C) for the light fraction (Fraction 2). A mechanical vacuum pump placed after the cold trap provided the vacuum condition for vacuum pyrolysis of biomass. The reactor system was evacuated at 0.09, 0.7 and 3 kPa (denoted as 1, 2 and 3) by vacuum pump (Edward RV3) under air atmosphere when temperature conditions were set to 350, 450 and 520°C at a heating rate of 20°C /min controlled by PID controllers under a vacuum condition. Biochar produced at certain temperature and pressure was named as B-temperature-pressure. For example, B-350-1 refers to the biochar produced at 350°C and 0.09 kPa. Pyrolysis condition is denoted as temperature-pressure. At the desired temperature, the system was maintained for 1 hour. Each vacuum pyrolysis was conducted three times at an experimental condition. As a control experiment, biochar was produced at a temperature of 350, 450 and 520°C under nitrogen atmospheric pressure condition. Biochar produced for the control experiment was named as B-temperature-N.

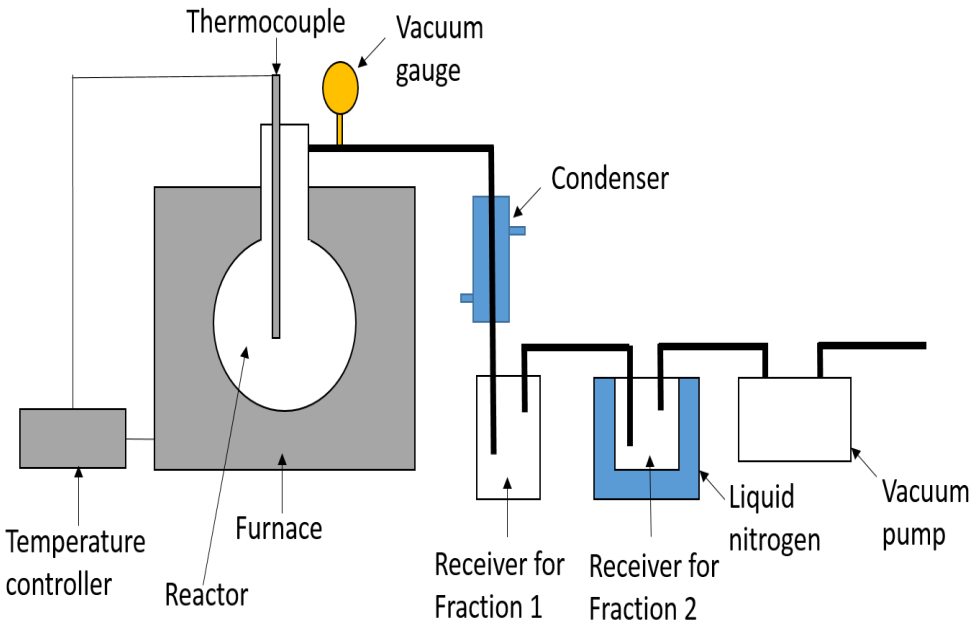

Figure 3. Scheme of the vacuum pyrolysis experimental setup

2.2.3 Characterization of biochar

The elemental composition of biochar was analyzed with an ultimate analyzer (Vario MICRO elemental analyzer). The proximate analysis of biochar was conducted following ASTM D3172[46]. The nitrogen adsorption isotherms of biochar were obtained by nitrogen (Airgas, 99.999%) adsorption at -196.15°C (NOVA 4200e). Biochar samples were degassed for 3 hours at 300°C. The BET surface area was calculated from the Brunnauer-Emmett-Teller (BET) equation[47]. The micropore volume was calculated by the Dubinin-Radushkevich (DR) equation[48]. The total volume was analyzed at a relative pressure of P/P_0 = 0.99. The mesopore volume was determined from the difference between total pore volume and micropore volume. The functional groups were

investigated by Fourier transform infrared spectroscopy (Shimadzu IRAffinity-1 FTIR). The spectra were recorded between 400 and 4000 cm^{-1} with a resolution of 4 cm^{-1}.

2.2.4 Methylene blue (MB) adsorption test

A 30 ppm methylene blue solution was prepared in deionized water. Each biochar, derived from vacuum pyrolysis and conventional pyrolysis, was submerged in solution at a ratio of 50 mg of biochar to 20 ml of solution. Each batch was shaken at 100 rpm for 24 hours. Then, the solution was filtered and the filtrate was collected. The absorbance of the filtrate was measured at 664 nm using UV-spectroscopy. The amount of MB adsorbed on the biochar at equilibrium q_e (mg/g) was calculated as:

$$q_e = V(C_o - C_e)/w \quad (1)$$

where C_o and C_e are the concentration of MB at initial and equilibrium. V is the volume of the MB solution, and w is the mass of dry biochar.

2.3 Results and discussion

2.3.1 Biomass characteristics

Table 1 shows the comparison of Ashe juniper characteristics to some typical feedstocks. The moisture content of Ashe juniper is higher than all the other raw materials listed: rice straw [49], corn stover [16], woodchip [50] and saw dust [51]. Similar to woodchip (0.3%) and sawdust (0.45%), Ashe juniper (0.6%) exhibited relatively lower ash content compared to other lignocellulosic biomass. Elemental analysis revealed that Ashe juniper comprised the highest carbon element content among the listed raw materials. It suggested

that Ashe juniper might be a promising precursor to develop carbon-based functional materials.

Table 1 Proximate and elemental analysis of raw materials

	Ashe juniper	Rice Straw	Corn Stover	Woodchip	Sawdust
Proximate analysis [a] (wt %)					
Moisture	11.7	7.3	7.27	10.0	8.78
Volatile	75.2	60.84	80.3	78.5	78.14
Fixed carbon	12.5	16.61	9.93	11.2	12.63
Ash	0.6	22.55	2.5	0.3	0.45
Elemental composition [b] (wt %)					
C	52.20	48.75	44.40	46.29	45.18
H	5.13	5.98	5.60	6.62	6.59
N	0.11	1.99	0.43	0.20	-
O	42.56	43.28	49.12	46.79	48.23
S	-	-	0.45	0.10	-

[a] Wet basis

[b] Dry ash-free basis

2.3.2 The complete characterization of the biochar

2.3.2.1 Proximate analysis

The influence of temperature and vacuum pressure on volatile matters, fixed carbon, and ash content in biochar was investigated. As shown in Table 2, biochar produced under vacuum conditions showed lower volatile combustible matter and ash contents while a higher fixed carbon content were obtained compared to biochar from conventional pyrolysis (B-350, 450 and 520-N) due to the higher severity of volatilization in vacuum condition. Biochar with high fixed-carbon content can be used as a reducing agent in the metallurgy industry[52]. Therefore, vacuum condition will be helpful for the production of biochar-metallurgical-reductants.

In the case of biochar samples from vacuum condition, volatile contents decreased from 55.9% to 22.5% as temperature increased from 350 to 520°C due to more volatilization occurring at a higher temperature. Conversely, the fixed carbon and ash contents increased as temperature increased. At higher vacuum pressure, more volatiles were probably removed, so that relatively higher fixed carbon and ash contents were obtained at 350 and 450°C. However, at 520°C, the increased vacuum pressure increased volatile contents and decreased fixed carbon and ash contents. This is consistent with studies reporting that increased absolute pressure higher than atmospheric pressure leads to higher fixed carbon in biochar because of the enhancement of the formation of coke from the tarry vapor[15, 22]. However, the high vacuum pressure in this study inhibited the conversion of some volatiles trapped in damaged porous structures into coke, yielding higher volatile contents and lower fixed carbon contents in B-520-1 and B-520-2

compared to B-520-3. Furthermore, the vacuum pressure may promote the release of ash from biochar due to decreased boiling point of ash, which resulted in lower ash contents in B-520-1 and B-520-2. The release of ash during pyrolysis at high temperature is a well-known phenomena[13]. Since, inorganic ash minerals cause the secondary charring reaction [13], the lower ash contents in B-520-1 and B-520-2 resulted in the higher volatile and lower fixed carbon contents due to the insufficient secondary charring reaction.

2.3.2.2 Elemental analysis

The effects of temperature and vacuum pressure on the elemental composition (C, H, N, and O) of biochar were investigated as shown in Table 2. B-520-2 showed the highest carbon contents (86.3%) compared to biochar produced from various raw materials. The coefficients of determination (r^2) were calculated to investigate the correlations between temperature, vacuum pressure and elemental composition as shown in Table 3. Over the entire range of temperature and vacuum pressure, the temperature term mainly affected the elemental composition based on coefficients of C, H and O (r^2=0.83, 0.81 and 82, respectively). The effect of temperature on nitrogen content (r^2=0.016) and the effect of vacuum pressure on nitrogen content (r^2=0.008) were negligible. Furthermore, there was a good correlation between temperature and elemental content (C, H, O) with r^2>0.89 at constant vacuum pressure. However, the severity of the effect of vacuum pressure on elemental compositions slightly varied at a constant temperature. Specifically, the C content increased and H and O contents decreased as vacuum pressure increased at 350°C (r^2 = 0.82 for C, 0.82 for H and 0.72 for O). A large

fraction of surface functional groups and volatiles in biomass are composed of O, N, and H. Hence, the decrease of H and O at 350°C was due to the surface functional groups and volatiles removal from the reactor and biomass at 350°C by an increased mean free path at the higher vacuum pressure condition. The correlation of vacuum pressure at the constant temperature of 450°C to the elemental data showed insignificant as r^2 for C, H and O was lower than 0.2. Conversely, the removal of N was significantly affected by vacuum pressure (r^2 for N =0.76). During atmospheric pyrolysis, N-containing volatiles are released at a temperature above 400°C[8, 53]. Therefore, the high vacuum pressure may facilitate the release of N-containing volatiles from biomass due to a greater mean free path of N-containing volatiles. At 520°C, the vacuum pressure was insignificant for C, H, N and O (r^2 <0.33). Additionally, at 450 and 520°C under 0.09 kPa, C content decreased and O increased slightly. This response might be related to the inhibition of secondary charring reaction of tar at the highest vacuum pressure (0.09 kPa)

Table 2 Proximate and elemental analysis of biochars

	Elemental analysis[a] *(wt %)*				Proximate analysis[b] *(wt %)*		
	C	H	N	O	Volatile	Fixed carbon	Ash
B-350-1	73.5±1.2	2.9±0.2	0.30	23.3±1.1	39.1±1.8	55.7±1.1	5.2±0.1
B-350-2	73.1±0.8	3.2±0.2	0.22	23.4±0.7	46.1±1.3	49.0±1.8	4.9±0.4
B-350-3	67.2±1.4	3.6±0.1	0.22	29.0±1.3	55.9±0.3	42.5±1.3	1.6±0.6
B-450-1	77.1±2.1	2.4±0.2	0.29	20.3±2.3	36.8±0.2	57.0±0.7	6.2±0.1
B-450-2	80.6±1.6	2.3±0.03	0.26	16.9±1.6	35.5±1.5	57.4±0.6	7.1±0.8
B-450-3	77.6±0.5	2.3±0.1	0.32	19.7±0.4	41.0±0.1	57.0±1.3	2.0±0.2
B-520-1	83.9±1.2	2.0±0.06	0.26	13.8±1.2	33.6±0.5	62.7±1.7	3.7±0.1
B-520-2	86.3±1.2	2.0±0.09	0.24	11.5±1.2	32.1±0.5	63.3±0.8	4.6±0.9
B-520-3	85.8±0.9	1.9±0.06	0.28	11.9±0.9	22.5±0.9	71.4±0.5	6.1±0.8
B-350-N	67.7±1.0	3.7±0.07	0.37±0.03	28.2±1.1	63.4±1.2	34.5±0.5	2.1±0.02
B-450-N	75.9±1.4	3.5±0.1	0.34±0.01	20.2±1.4	53.4±1.8	44.3±1.6	2.3±0.5
B-520-N	78.8±0.9	3.0±0.06	0.33±0.06	17.8±0.9	41.9±1.8	55.5±1.0	2.6±0.3
Rice straw[49]	81.4	2.3	1.1	15.1	10.61	38.72	50.7
Wood chip[54]	85.6	2.84	0.09	9.86	-	-	1.64
Cotton straw[55]	79.6	4.3	1.3	14.8	-	-	-
Pine wood[56]	83.7	3.6	0.1	14.8	25.2	72.7	2.1

[a] Dry ash-free basis [b] Dry basis

Table 3 Coefficient of determination (r^2) between temperature, pressure, and elements

	C	H	N	O
Temperature	0.83	0.81	0.016	0.82
Pressure	0.017	0.038	0.008	0.015
Temperature at 0.09 kPa	0.89	0.93	0.33	0.82
Temperature at 0.7 kPa	0.93	0.91	0.40	0.93
Temperature at 3 kPa	0.98	0.95	0.39	0.98
Pressure at 350°C	0.82	0.82	0.30	0.72
Pressure at 450°C	0.001	0.24	0.76	0.001
Pressure at 520°C	0.13	0.13	0.33	0.14

2.3.2.3 The degree of aromaticity of biochar

Using the Van Krevelen plot for H/C and O/C molar ratio, the effect of temperature and vacuum pressure on the degree of the aromaticity of biochar was investigated[57]. Low H/C and O/C molar ratio indicates the relatively highly developed aromatic characteristic in biochar. As shown in Figure 4 and Table 4, the degree of aromaticity increased with increasing pyrolysis temperature. However, the vacuum pressure showed different effects on the degree of aromaticity at each temperature. To be specific, at 350°C, the degree of aromaticity was enhanced with increasing vacuum pressure because a higher vacuum pressure promoted the removal of oxygen contained materials in biomass, which resulted in lower H/C and O/C molar ratios of B-350-1 and 2 compared to that of B-350-N. At 520°C, increasing vacuum pressure leads to the relatively lower degree of aromaticity. At

450°C, the degree of aromaticity increased when the vacuum pressure increased from 3 to 0.7 kPa while the aromaticity decreased at the vacuum pressure of 0.09 kPa. However, the effect of vacuum pressure on the elemental ratios at 450 and 520°C was not significant compared to the results at 350°C. The relatively higher temperature induced easier removal of vapors from the reactor and secondary charring reaction offsetting vacuum pressure effect. Nevertheless, B-450-2 and B-520-1, 2, 3 had lower H/C and O/C molar ratio values than B-450 and 520-N because of easier removal of vapors under vacuum conditions. Furthermore, H/C and O/C ratio of B-520-3 are lower than biochar derived from various biomasses as shown in Table 4, indicating the most carbonized biochar was produced under 520°C and 3 kPa condition. Especially, biochar produced at relatively less severe condition (B-350-1) had a lower H/C molar ratio values than biochar derived from other biomasses at a higher temperature (450 and 500°C) except for rice straw, corn stover and wood chip as shown in Table 4. Therefore, the vacuum pressure as well as temperature are both influential factors for controlling aromaticity of biochar. It is suggested that biochar with a O/C<0.4 and H/C<0.6 will be effective carbon sequestration agents in soil [58]. The result showed that all prepared biochar samples under vacuum conditions except for B-350-3 have the potential for application as carbon sequestration agent. It means that carbon sequestration agents can be energy-efficiently produced from Ashe juniper using lower temperature vacuum pyrolysis process (350°C and 0.09 or 0.7 kPa). Especially, B-520-3 is expected to be most stable in soil due to the lowest O/C and H/C. Furthermore, biochar is well documented as a potential precursor material that can be used as catalyst supports due to high carbon contents, highly developed aromaticity and surface functional

groups which act as an active site to form metal catalyst on the surface of biochar[8, 9]. Highly carbonized biochar with surface functional groups might have potential as a catalyst support. B-450-1, 2 and 3 with high carbon contents and highly developed aromaticity are presumably adequate catalyst support compared to B-520-1, 2 and 3 due to higher O/C and (O+N)/C which are parameters related to surface functional groups.

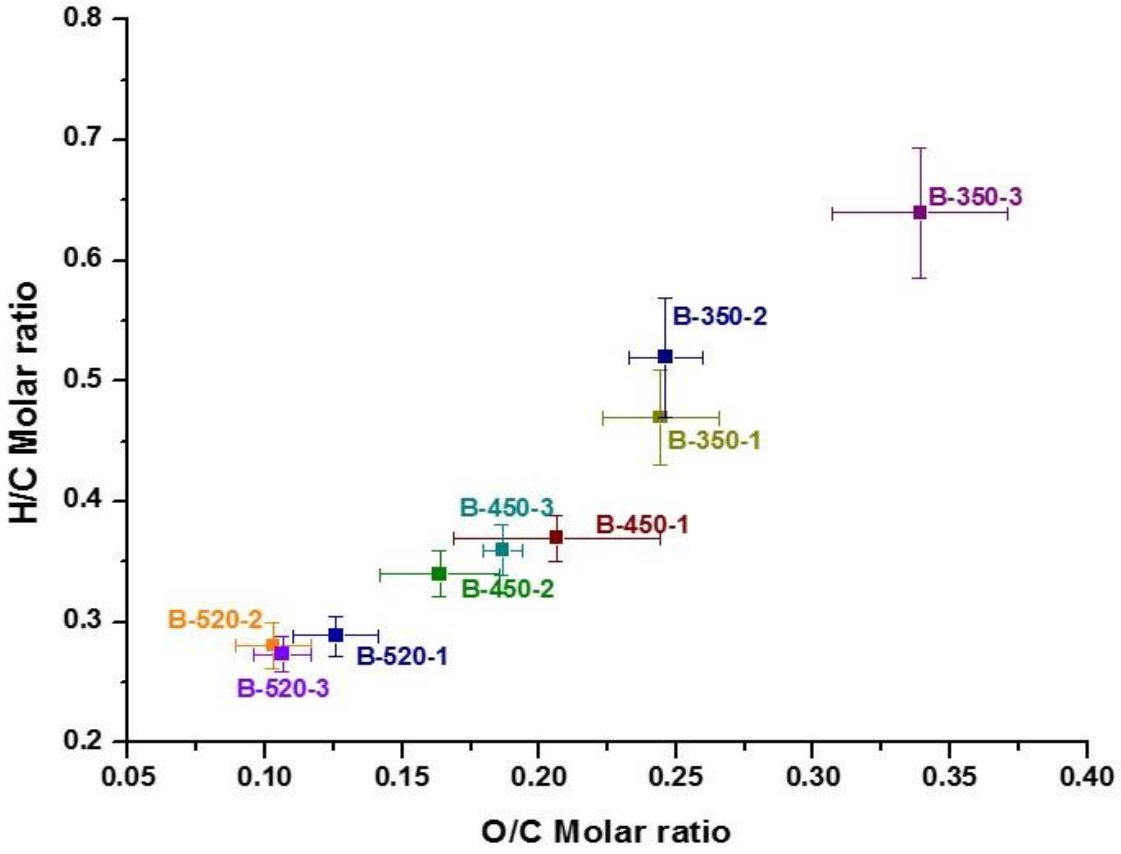

Figure 4. Van Krevelen plot for biochars derived at different pyrolysis conditions

Table 4 The data of pyrolysis temperature and H/C and O/C ratio of biochars

Biochar	Pyrolysis temperature	Molar ratio		
		H/C	O/C	(O+N)/C
B-350-1	350°C	0.47	0.24	0.24
B-350-2	350°C	0.52	0.24	0.24
B-350-3	350°C	0.64	0.32	0.33
B-450-1	450°C	0.37	0.20	0.20
B-450-2	450°C	0.34	0.16	0.16
B-450-3	450°C	0.36	0.19	0.22
B-520-1	520°C	0.28	0.12	0.13
B-520-2	520°C	0.27	0.10	0.10
B-520-3	520°C	0.27	0.11	0.11
B-350-N	350°C	0.66	0.31	0.32
B-450-N	450°C	0.55	0.19	0.20
B-520-N	520°C	0.46	0.17	0.17
Rice straw[49]	500°C	0.34	0.14	-
Corn stover[16]	500°C	0.38	0.06	-
Wood chip[54]	500°C	0.4	0.09	-
Sawdust[51]	500°C	0.54	0.44	-
Rice husk[59]	500°C	0.63	0.22	0.23
Cotton straw[55]	450°C	0.65	0.14	0.15
Poplar wood[60]	460°C	0.60	-	-
Pine wood[56]	500°C	0.52	0.13	0.13
Maize straw[61]	500°C	0.48	0.13	0.15
Sugarcane[61]	500°C	0.61	0.17	0.18

2.3.2.4 FTIR Analysis

FTIR results, shown in Figure 5, confirmed that the aromaticity of biochar was improved with increased pyrolysis temperature. However, pressure conditions had no effects on the surface structures. Peaks in the range of 690-900 cm^{-1} indicate C-H bend in aromatic groups[19, 62, 63]. These peaks were observed probably due to the improvement of aromaticity of biochar with the increased pyrolysis temperature. Broad peaks and some peaks between 1030 cm^{-1} and 1411 cm^{-1} correspond to carboxylic acids, derivates and amines[19]. The decreased intensity of these peaks with increased pyrolysis temperature means the removal of oxygen and nitrogen from biomass. This result corresponds to elemental analysis results. The peak at 1420 cm^{-1} indicates aromatic C-C ring stretching [64]. The intensity of this peak also decreased with the increased pyrolysis temperature due to the improvement of the degree of aromaticity (Figure 4 and Table 4). The peak at around 1600 cm^{-1} corresponds to the presence of aromatic C=O ring stretching or C=C stretching of aromatic groups in lignin[65]. Thus, the decreased intensity of this peak with the increased pyrolysis temperature means the further decomposition of lignin with the increased pyrolysis temperature.

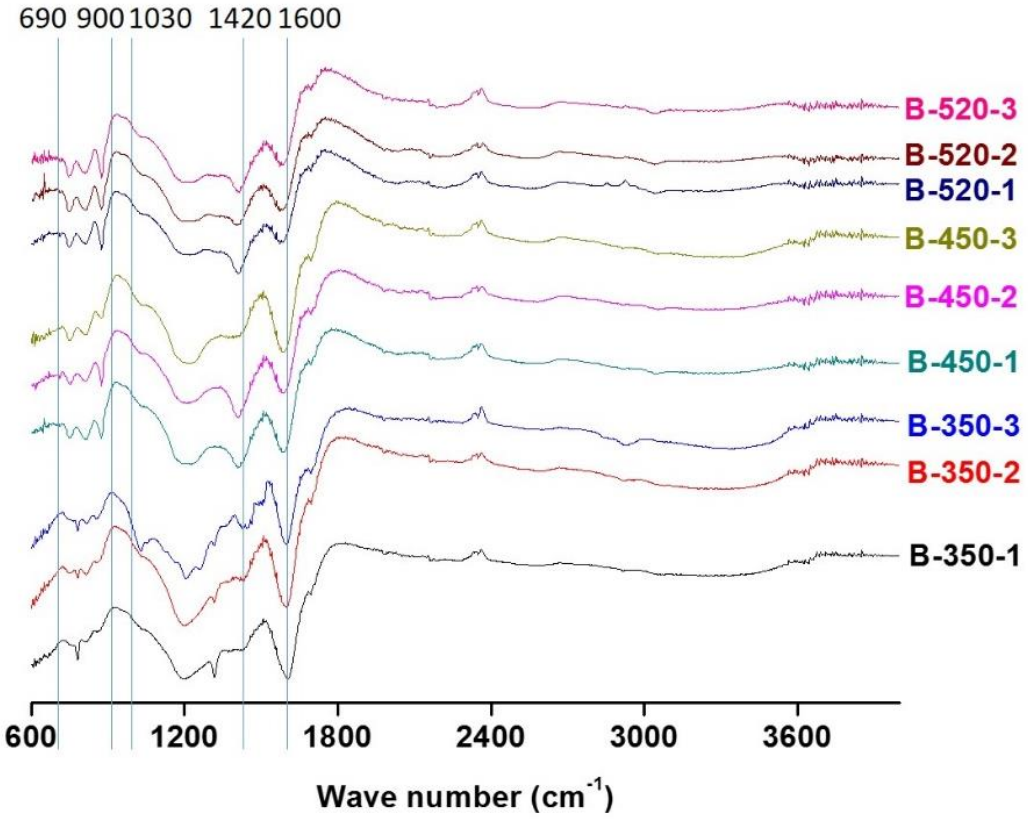

Figure 5. FTIR spectra of biochars obtained at different pyrolysis conditions

2.3.2.5 Effects of the processing parameters on porous structures

The effect of temperature and vacuum pressure on the textile structures of biochars was investigated through N_2 isotherm analysis. As shown in Figure 6, for all biochar except for B-350-3, a sharp initial uptake was observed at low relative pressures (p/p^o) indicating the development of microporosity. Except for biochar produced at 350°C, the isotherm of all biochar showed a gradual uptake of N_2 with increasing relative pressure on biochar, suggesting the coexistence of micropores and mesopores.

As shown in Table 5, S_{BET}, V_{total}, V_{micro} and V_{meso} of biochars increased with the increased temperature. B-520-3 showed the highest surface area with 560.2 m^2/g and B-350-3 showed the lowest surface area with 4.1 m^2/g. The increased S_{BET}, V_{total}, V_{micro} and V_{meso} probably correlated with increasing volatiles removal from biomass with increasing pyrolysis temperature. On the other hand, S_{BET}, V_{total}, and V_{micro} of biochar produced under N_2 atmospheric pressure were much smaller than biochar from vacuum pyrolysis due to the inhibition of the formation of microporosity by clogging of pores with trapped tar and coke from the secondary charring reaction. Therefore, the vacuum pressure is a crucial parameter to develop microporous structures. Moreover, the surface area of B-520-3 was about 1.5 times to 69 times larger than reported biochars as shown in Table 5.

At 350°C, vacuum pressure had a positive effect on the development of porosity. S_{BET}, V_{total} and V_{micro} of B-350-1 were approximately 174%, 103% and 121% larger than B-350-2 probably due to the accelerated volatile removal from biomass at higher vacuum pressure. At 450°C, S_{BET}, V_{total}, V_{micro} and V_{meso} increased with increasing vacuum pressure from 3 kPa to 0.7 kPa but decreased at 0.09 kPa. At 520°C, S_{BET} decreased with increasing vacuum pressure from 3 kPa to 0.09 kPa while V_{total}, V_{micro} and V_{meso} decreased from 3 kPa to 0.7 kPa but increased at 0.09 kPa. The decrease of S_{BET} is probably due to the blockage of pores by condensed volatiles, which were not decomposed or converted into coke by a secondary reaction. In addition, the violent volatilization under the highest vacuum pressure at high temperature may damage porous structures[66]. Furthermore, at high temperature, S_{BET} and pore volume may be decreased by the heat shrinkage of the carbon structure[67]. At 450 and 520°C, carbon backbone may not be rigid. Therefore, the

structure of char can be damaged vigorously by the violent evaporation of volatiles at negative pressure. The development of mesoporosity of B-520-1 was also probably due to the collapsed microporous structures by violent evaporation and heat shrinkage of carbon structure[66].

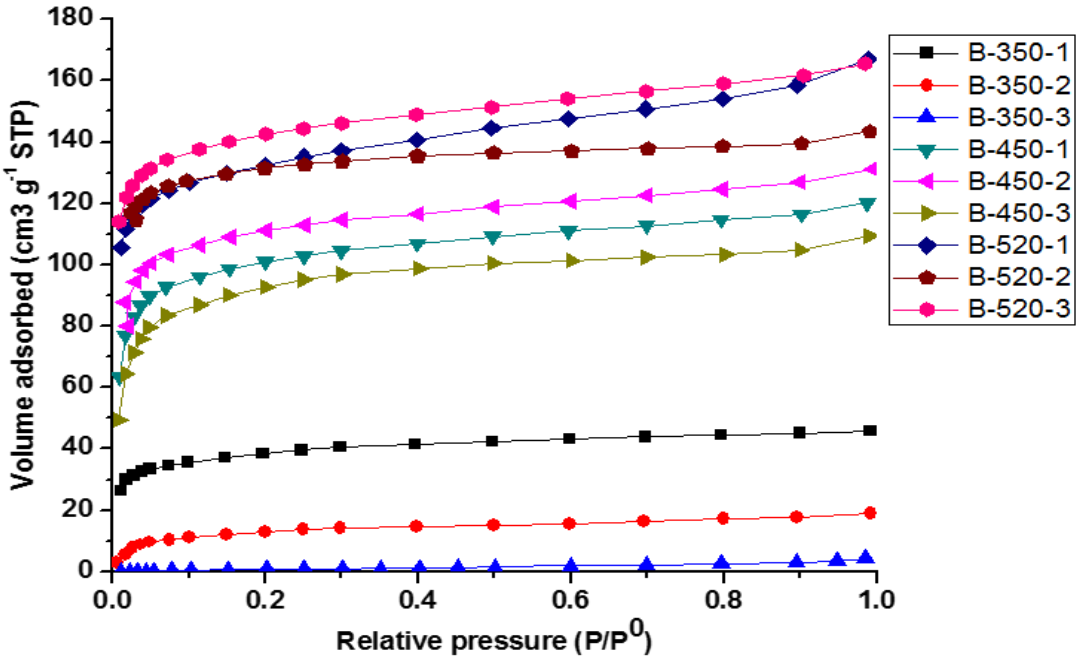

Figure 6. Nitrogen adsorption isotherm of biochars obtained at different pyrolysis conditions

2.3.2.6 Methylene blue (MB) adsorption test

Produced biochar can be a good adsorbent due to well-developed porosity and surface area. To test this hypothesis, MB adsorption on biochar at equilibrium (q_e) was

investigated as shown in Table 5. The biochar samples produced under vacuum condition had a relatively higher MB adsorption than the biochar samples produced under N_2 atmospheric pressure (B-350-N, B-450-N and B520-N). This is probably due to the well-developed porosity of biochars produced by vacuum pyrolysis. Regardless of vacuum pressure conditions, the MB adsorption of biochar increased with increasing pyrolysis temperature from 350 to 450°C. However, the biochar produced at 520°C showed a decreased MB adsorption compared to biochar at 450°C. Also, vacuum pressure affected MB adsorptivity of biochar produced at each pyrolysis temperature. At 350°C, the biochar produced from higher vacuum pressure showed a higher adsorption capacity probably due to the increased surface area and pore volume. At 450°C, B-450-2 showed higher MB adsorption than B-450-1 and B-450-3 in accordance with the changes of the surface area of biochar. At 520°C, sample B-520-2 showed the lowest MB adsorption probably due to lower pore volume compared to B-520-1 and B-520-3 as shown in Table 5. Sample B-450-2 showed the highest adsorption of methylene blue with 6.8 mg/g, suggesting the most prominent absorbent among the tested biochars in terms of the removal of MB. Even though, biochar samples produced at 520°C had higher surface area and pore volume, these sample's adsorption capacity was lower than B-450-1, 2 and 3. Therefore, we assume that there are specific interaction between biochar and MB affecting the adsorption of MB other than textural properties due to a non-direct relationship between the adsorption capacity and the textural properties. The cation exchange capacity of biochar or electrostatic interactions between biochar and MB might be factors affecting the adsorption capacity[68, 69]. Further investigation regarding specific interaction is required.

Table 5 Textural properties and q_e of biochars obtained at different process conditions

	S_{BET} (m^2/g)	V_{total} (cm^3/g)	V_{mic} (cm^3/g)	V_{meso} (cm^3/g)	AV[a] (nm)	q_e[b] (mg/g)
B-350-1	144.7±5.2	0.072	0.062	0.0097	0.98	1.55±0.13
B-350-2	53.2±3.0	0.038	0.028	0.0095	1.11	1.10±0.22
B-350-3	4.1±0.1	0.0069	0.001	0.0057	3.35	0.76±0.29
B-450-1	395.4±16.1	0.20	0.17	0.029	0.94	2.89±0.11
B-450-2	441.7±22.0	0.22	0.19	0.032	0.92	6.80±0.27
B-450-3	364.4±26.3	0.17	0.16	0.012	0.93	3.29±0.36
B-520-1	516.2±8.4	0.27	0.21	0.056	1.00	2.88±0.24
B-520-2	529.4±13.0	0.23	0.21	0.016	0.84	1.52±0.26
B-520-3	560.2±9.1	0.25	0.22	0.034	0.92	2.27±0.24
B-350-N	9.7±0.2	0.012	0.002	0.010	2.42	0.57±0.028
B-450-N	10.8±1.9	0.015	0.002	0.013	2.86	0.48±0.050
B-520-N	22.7±0.7	0.028	0.002	0.026	2.43	0.48±0.13
Corn stover[16]	185	-	-	-	1.00	-
Wood Chip[54]	312	-	-	-	-	-
Softwood[70]	383.7	-	0.196	-	-	-
Hardwood[70]	372.8	-	0.155	-	-	-
Pine wood[56]	392	-	-	-	-	-
Rice husk[59]	34.4	0.028	-	-	-	-
Cotton straw[55]	367.1	-	-	-	-	-
Maize straw[61]	33.2	-	-	-	-	-
Sugarcane[61]	97.8	-	-	-	-	-

[a] The average pore radius [b] The methylene blue adsorption at equilibrium

2.4 Conclusions

The effect of temperature and vacuum pressure on vacuum pyrolysis of Ashe juniper was investigated. Pyrolysis temperature and vacuum pressure had a significant impact on tailoring elemental composition, the degree of carbonization, surface functionality, proximate analysis, and textile properties of biochar. Specifically, developed biochar showed a higher degree of carbonization and surface area compared to reported biochar. A biochar with lower H/C ratio can be produced from Ashe juniper at a lower temperature with the effect of vacuum pressure. This is a valuable improvement over biochar reported in literatures. B-520-3 is expected as a carbon sequestration agent due to the relatively higher stability in soil for the reduction of total greenhouse gas emissions from the soil and carbon storage in the soil. B-450-1, 2, and 3 achieved good catalyst support properties due to their highly developed aromaticity and surface functionality. To investigate the suitability of the biochar as adsorbents, MB adsorption tests were performed. Sample B-450-2 showed the highest MB adsorption with approximately 6.8 mg/g.

CHAPTER III

THE PRODUCTION OF FUNCTIONALIZED ASHE JUNIPER DERIVED-BIOCHAR AS THE PROMISING ADSORBENT WITH HIGH DYE REMOVAL EFFICIENCY

3.1 Introduction

The disposal of dye used in industries such as textiles, paper, rubber, paints, printing, etc., can eventually seriously damage the environment due to their toxic, mutagenic, and carcinogenic properties[27]. Currently, conventional water treatment methods that use light, oxidization agents, and anaerobic digestion, cannot decompose many textile dyes efficiently due to high resistance of dye chemicals[71]. However, the adsorption process has been regarded as an effective and attractive process for the removal of dye contaminants[25, 71]. For example, an adsorption process using activated carbon—normally derived from coal—has been widely used as the most efficient process to remove dye chemicals from water. However, the production cost of activated carbon limits its practical applications[26]. Therefore, the development of adsorbents with low production costs is crucial for practical applications in the adsorption process.

Biochar is a carbon-rich and porous solid material. Recently, biochar has attracted increasing attention as a carbon sequestration agent due to its ability to mitigate greenhouse gas emissions[11, 12]. It also has applications as a soil amendment capable of improving soil health[11, 12] and biochar has demonstrated its potential as a contaminant adsorbent, carbon catalyst, and catalyst support[8, 9]. Biochar has optimistic potential for use

as an adsorbent for the removal of contaminants such as in water purification processes by absorbing hydrocarbons, other organics, and some inorganic metal ions[17, 25]. Furthermore, biochar requires less investment than activated carbon[26]. Therefore, biochar is expected to be utilized as a low-cost adsorbent in water treatment alternatives to activated carbon[26].

Biochar has shown promising results in the removal of dye materials[17]. However, biochar has low adsorption capacities compared to conventional adsorbents and investigations have conducted at concentrations lower than 200 mg/L[17, 25, 27]. This means that there are some hurdles to overcome in the commercialization of biochar as an adsorbent due to its relatively low adsorption capacity and removal efficiency. In practical applications, the adsorption capacity of biochar should be reliable even at concentrations higher than 300 mg/L which is practically the final dye concentration in effluents[27]. Therefore, biochar with a high adsorption capacity for high dye concentrations should be developed for biochar's practical applications in waste water treatment.

Surface functionalization is presumably one way of improving the utility of biochar as an adsorbent[8, 25]. When developing usable biochar for the removal of high concentration dye chemicals, surface oxidation is one method by which particular functionalities such as oxygen-containing functional groups can be anchored to the biochar[8, 25]. Many reports have revealed ways of functionalizing the surface of biochar such as sulfonation and partial oxidation to produce surface functionalized biochar with improved affinity for particular contaminants[8, 25].

There has been no study on the functionalization of biochar derived from Ashe juniper waste for adsorption process to the best of our knowledge. Ashe juniper has spread rapidly, altering both rangeland plant communities and the hydrological landscape. Management with hydraulic shears or bulldozers for the removal of Ashe juniper might produce a significant quantity of Ashe juniper waste. However, Ashe juniper waste, which has relatively high carbon content, is a good candidate biomass for the production of high-quality biochar. Therefore, the main objective of this research is converting Ashe juniper waste into a functionalized biochar with a high adsorption capacity on dye chemicals for the valorization of Ashe juniper waste. For adsorption study, methylene blue (MB) and methyl orange (MO) were selected as model dye contaminants due to their wide application and toxicity to human such as cyanosis and tissue necrosis[69, 72]. The specific objectives are as follows:

a. Characterize the effects of the acid concentration on the physicochemical properties of functionalized biochar,
b. Investigate the effects of acid treatment conditions and the properties of functionalized biochar on adsorption capacity for methylene blue,
c. Optimize and develop a model for adsorption capacity of methylene blue on functionalized biochar,
d. Demonstrate the adsorption mechanism through adsorption isotherm and kinetic studies, and
e. Confirm the selectivity of functionalized biochar to methylene blue from dye mixture solutions.

3.2 Materials and methods

3.2.1 Material

Ashe juniper was obtained from thinning in Hills Country (TX, USA). Sample preparation, the proximate analysis and elemental composition of Ashe juniper are available in Chapter 2.

3.2.2 Preparation of biochar

The Ashe juniper was dried for 2 h prior to pyrolysis, in which the dried Ashe juniper was pyrolyzed under a nitrogen atmosphere. The information about our apparatus is available in our previous report. For each experiment, 10 g of the raw biomass was placed in a glass flask (Chemglass) before insertion into an electric furnace. The main flask was connected to a condenser for the collection of the bio-oil. 450°C for pyrolysis was seleceted as biochar produced at the temperature had the lowest adsroption capacity as shown in Table 5 and less heat was consumed than 520°C for production of biochar. The reactor system was heated to 450°C in nitrogen atmospheric pressure condition at a heating rate of 20°C/min, controlled by PID controllers, and the system was maintained at the desired temperature for one hour.

3.2.3 Acid treatment of biochar

Biochar samples were treated with H_2SO_4 solution at different concentrations; 10 g of dried biochar samples were mixed with 100 ml of 50, 70, and 90% H_2SO_4 solution

for 1.5 h at 120°C. After acid treatment, samples were washed with deionized water until the pH was close to neutral and washed samples were then dried at 105°C in an oven. The prepared samples were named B-0, B-50, B-70, and B-90, respectively. The numbers refer to the biochar's treatment with 0, 50, 70, and 90% H_2SO_4 solution.

3.2.4 Characterization of biochar

An ultimate analyzer (Vario MICRO elemental analyzer) analyzed the elemental composition of the acid-treated biochar. The nitrogen adsorption isotherms of the biochar were obtained by nitrogen (Airgas, 99.999%) adsorption at -196.15°C (NOVA 4200e). Biochar samples were degassed for three hours at 300°C. The BET surface area was calculated from the Brunnauer–Emmett–Teller (BET) equation[47] and the micropore volume was calculated by the Dubinin–Radushkevich (DR) equation [48]. The total volume was analyzed at a relative pressure of $P/P_0 = 0.99$. The mesopore volume was determined from the difference between the total pore volume and the micropore volume. The surface functional groups were investigated by Fourier transform infrared spectroscopy (Shimadzu IRAffinity-1 FTIR). The spectra were recorded between 400 and 4000 cm^{-1} with a resolution of 4 cm^{-1}.

3.2.5 Adsorption experiments in a single system

Certain concentrations of methylene blue (MB) solution were prepared in deionized water. The pH value of the solutions was adjusted by adding 0.1 M HCl and 0.1 M NaOH solution. In the batch adsorption test, 10 mg of acid-treated biochar sample was

submerged in 20 ml of solution to perform the adsorption study. Each batch was shaken at 200 rpm and 298 K for 72 hours in a shaking incubator. Then, the solutions were centrifuged and the supernatants were collected. The residual concentration of MB in the supernatant was measured using a UV-VIS spectrophotometer at a maximum wavelength of 664 nm. The amount of MB adsorbed on the adsorbents at equilibrium, Q_e (mg/g), was calculated as:

$$Q_e = \frac{V(C_0 - C_e)}{w}$$

where C_o and C_e (mg/L) are the concentrations of MB at initial and equilibrium points. V is the volume of the MB solution and w is the mass of the dry adsorbents.

3.2.6 Effect of initial MB concentration and adsorption equilibrium isotherm

MB solutions with different initial concentrations (100–500 mg/L) were mixed with 10 mg biochar samples. After 72 h of shaking at 200 rpm and 298 K, the equilibrium concentration of MB was measured using a UV-VIS spectrophotometer. Based on the equilibrium data, Langmuir isotherm and Freundlich isotherm models, which are given below, were employed to analyze the adsorbate–adsorbent interaction.

$$Q_e = \frac{Q_m K_L C_e}{1 + K_L C_e}$$

$$Q_e = K_F C_e^{1/n}$$

where Q_e is the adsorbed amount of MB per unit weight of adsorbent (mg/g) at the equilibrium concentration of MB (C_e, mg/L), K_L and K_F are the Langmuir and Freundlich constants, Q_m is the maximum adsorption capacity of MB (mg/g) for the adsorbents and n

is the heterogeneity factor. The term 1/n is a measure of the adsorption intensity or surface heterogeneity[73]. A value of 1/n closer to zero means that the surface has greater heterogeneity[73].

3.2.7 Adsorption kinetic

In the adsorption kinetic experiments, 30 mg of biochar was added to 20 ml of 300 ppm solution. The pHs of three solutions were respectively adjusted to 3, 6, and 10 to investigate the pH effect on the adsorption kinetic. Adsorption tests were performed at 298 K in a shaking incubator. At a specific time, the solutions were collected and centrifuged. The residual concentration in the supernatant was measured at 664 nm using a UV-VIS spectrophotometer; the amount of adsorbed MB on the biochar at different time intervals, Q_t (mg/g), was calculated as:

$$Q_e = \frac{V(C_0 - C_t)}{w}$$

where C_o and C_t (mg/L) are the concentrations of MB at the initial and at time t. V is the volume of the MB solution and w is the mass of dry adsorbents.

Pseudo-first order, Pseudo-second order, Nth order, and intra-particle diffusion kinetic models, which were expressed as follows, were employed to evaluate the adsorption rate controlling mechanism.

$$\frac{dQ_t}{dt} = k_1(Q_e - Q_t)$$

$$\frac{dQ_t}{dt} = k_2(Q_e - Q_t)^2$$

$$\frac{dQ_t}{dt} = k_3(Q_e - Q_t)^n$$

$$Q_t = k_i t^{1/2} + C$$

Where Q_t (mg/g) and Q_e (mg/g) are the amounts of MB adsorbed at time t (min) and equilibrium, respectively, and k_1 (min^{-1}), k_2 (g/(mg min)), k_3 $(g/mg)^{n-1}/min$) and k_i ($mg/(g\ min^{1/2})$) are the first-order, second-order, Nth-order and intraparticle diffusion rate constant.

3.2.8 Resonance surface methodology

A Box–Behnken design and regression analysis were selected for the optimization of adsorption capacity of biochar adsorbents on MB. The selected variables were the dosages of adsorbents, the initial concentrations of MB and the pH of each at three levels coded as +1, 0, and -1 for high, middle, and low values, respectively. Each variable's interaction effect of each variable was studied. JMP was used to formulate the experimental design and analyze the obtained data.

3.2.9 Adsorption experiment in a binary system

The adsorption of a methyl orange (MO) and methylene blue (MB) mixture on biochar was conducted at 298 K, 200 rpm for 72 hours. Various MB:MO ratios (250:50 ppm, 250:125 ppm, 250:250 ppm, and 250:500 ppm) were tested and the solution was diluted to remove the influence of each dye from the detection of the other after adsorption.

The concentrations of MO and MB were determined at 464 nm and 664 nm using a UV–VIS spectrophotometer.

3.3 Results and discussion

3.3.1 The characterization of functionalized biochar and the effect of acid concentration

The effect of the concentration of sulfuric acid on the physicochemical properties (elementary composition, textural properties, and surface functionality) was investigated. Table 6 shows the elemental composition of each prepared sample. Compared to raw biochar samples, acid-treated biochar samples had higher oxygen and sulfur content and lower carbon content. Furthermore, biochar samples treated with sulfuric acid showed higher O/C and S/C ratios than raw biochar samples. These results mean that the sulfuric acid altered the chemical properties of biochar. Furthermore, a higher O/C ratio was confirmed for a higher sulfuric acid concentration. The O/C ratio is highly related to the surface functionality; a higher O/C ratio indicates that higher oxygen contained functional groups were introduced on the biochar surface during acid treatment[68]. The higher S/C ratio was highly related to sulfonation on the surface of the biochar[74]. Sulfuric acids have been widely used to prepare solid acid materials through the sulfonation of the surface of the materials[8, 74]. The introduction of sulfonated groups on the surface of our samples was proved by FTIR measurement, as shown in Figure 7.

In addition, Figure 7 also shows that FTIR spectroscopy reveals the surface functional groups of each sample. Compared to raw biochar, we confirmed that the sulfonated groups, which are shown at 1032 cm^{-1} [74], were anchored on the surface of the

biochar (B-50, B-70, and B-90) after acid treatment. This observation is consistent with the increasing S content shown in elemental analysis. Furthermore, the ether groups, which are shown at 1151 cm^{-1} [75], were produced on the surface of B-50, B-70, and B-90, while untreated biochar had no ether groups. These functional groups were expected to act as active sites and adsorb the MB.

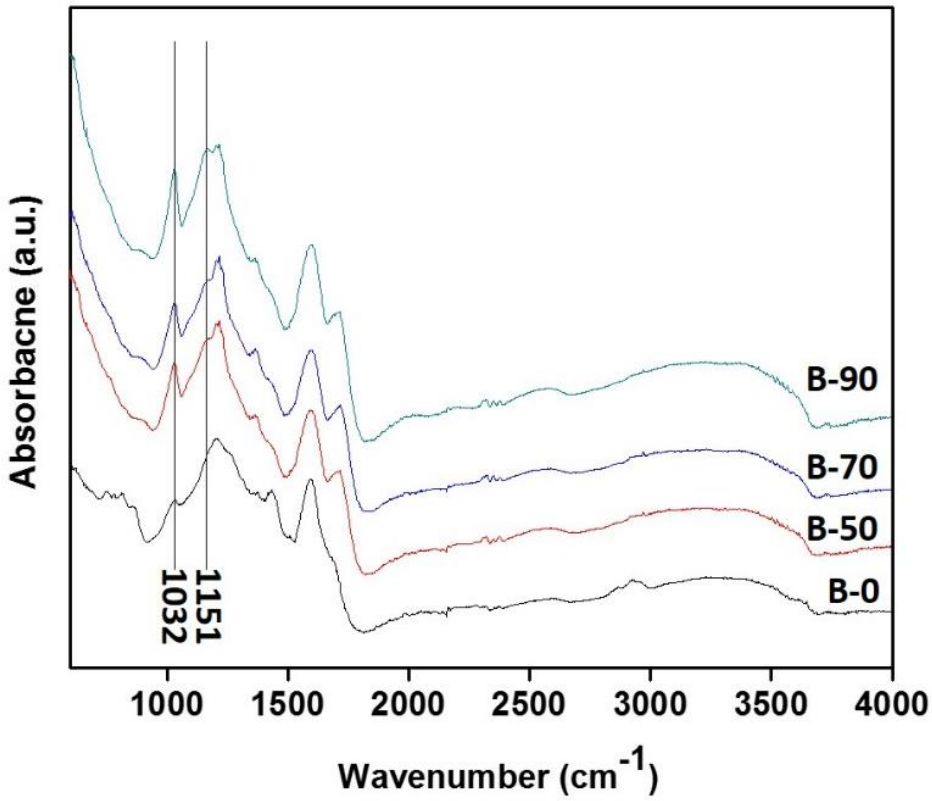

Figure 7. FTIR spectra of B-0, B-50, B-70, and B-90

Table 6. Elemental analysis and H/C, O/C, and S/C molar ratio

	Elemental analysis *(wt %)*							
	C	H	N	O	S	H/C	O/C	S/C
B-0	75.9 ± 1.4	3.5 ± 0.1	0.34 ± 0.01	20.2 ± 1.4	0	0.55	0.19	0
B-50	59.3 ± 0.9	3.0 ± 0.05	0.36 ± 0.02	36.7 ± 0.9	0.6 ± 0.03	0.61	0.47	0.013
B-70	57.0 ± 0.3	3.2 ± 0.04	0.31 ± 0.01	38.4 ± 0.2	1.1 ± 0.03	0.66	0.50	0.019
B-90	53.9 ± 0.5	3.5 ± 0.02	0.27 ± 0.03	40.5 ± 0.6	1.8 ± 0.05	0.77	0.56	0.029

The N_2 isotherm curves are presented in Figure 8. The curves for B-50, 70, and 90 are typical type 1—indicating microporosity—while the curves for the raw biochar represent macroporosity. The result means that the acid helps produce microporosity on the biochar samples. The results correspond with previous reports[76]; Table 7 lists the textural properties obtained from N2 isotherm data. As the concentration of sulfuric acid increased, the surface area of the acid-treated biochar samples decreased. B-50 had the highest surface area of 511 m^2/g, which was 50 times higher than for raw biochar. The pore volumes of the acid-treated samples also increased after acid treatment. Sulfuric acid might remove the volatiles condensed in the pores of the raw biochar resulting in the introduction of the porosity of the acid-treated biochar samples[8, 76]. However, the acid treatment condition became harsher for higher sulfuric acid concentrations; this probably leads to the degradation of the porous structures resulting in decreased surface area and pore volume. Besides, the higher degree of surface functional groups, which derived from

a higher concentration of sulfuric acid, might block pores and thus inhibit the development of higher surface area and pore volume[76].

The higher adsorption capacity from these acid treated biochars than the raw biochar was expected because of the higher surface area and the higher degree of surface functionality. MB adsorption tests were performed to confirm this hypothesis

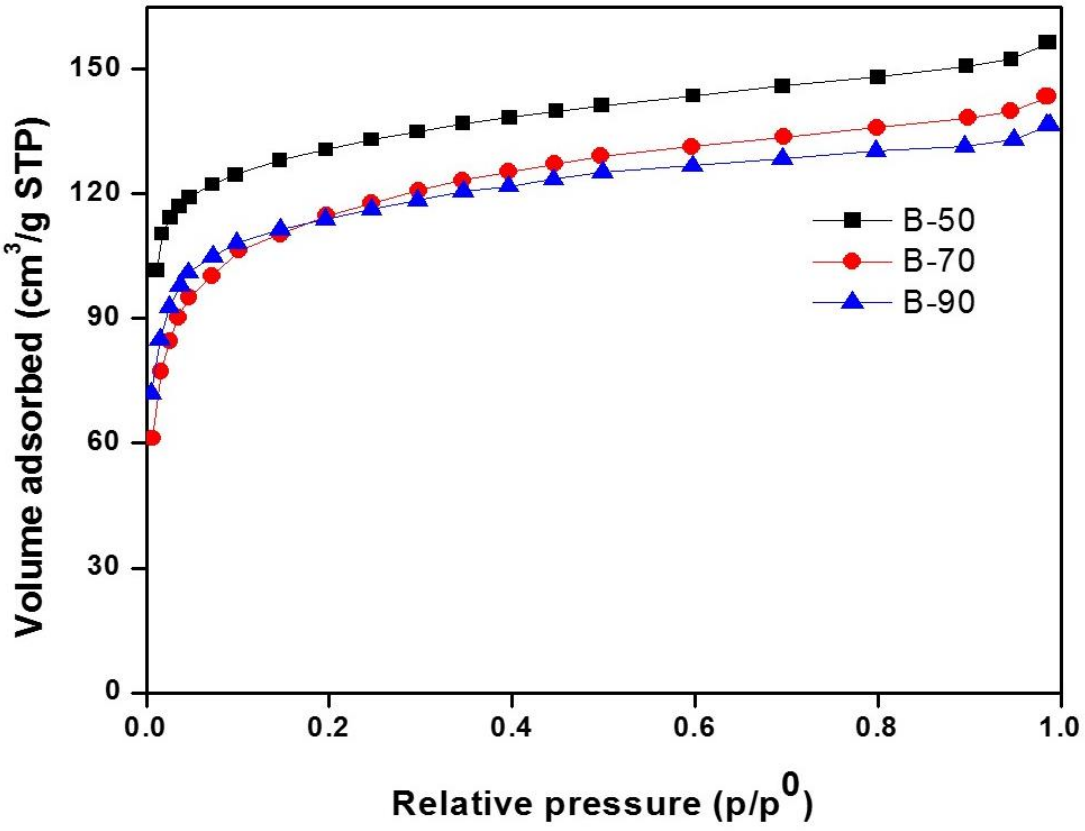

Figure 8. Nitrogen isotherm for B-50, B-70, and B-90

3.3.2 MB adsorption test

The effect of the concentration of sulfuric acid in treatment on the adsorption capacity of functionalized biochar on MB was investigated. As seen in Figure 9a), functionalized biochar showed higher adsorption capacity than raw biochar, as we expected, and the adsorption capacity of the biochar increased as the sulfuric acid concentration increased. B-90 had a higher adsorption capacity than both B-50 and B-70. Also, the increased sulfuric acid improved the surface area- normalized adsorption capacity (Q_{SA}) from 0.30 to 0.97 mg/m^2 and the ratio of adsorption capacity to (S+O)/C molar ratio from 324.27 to 714.53 mg/g. This result means that the highest adsorption capacity of B-90 was due to the synergistic effects of the high surface area and oxygen-contained surface groups such as sulfonated groups and carbonyl groups, as supported by Figure 7 and Table 7. Newly developed functional groups on the biochar surface contributed negative charges or polarity to the biochar surface[68, 76]. Therefore, negatively charged surfaces preferably attracted MB, which is a cationic chemical. A high surface area provided more active sites with which MB could interact. Although B-50 and B-70 showed lower adsorption capacities than B-90, the values of both biochars were higher than the reported values. B-90 was selected for further experiments to optimize the adsorption condition.

3.3.3 The optimization of adsorption capacity using the Box–Behnken method

The adsorption capacity was optimized, and the effect of each experimental parameter was investigated (initial pH, dosage, and initial MB concentration) on the

adsorption capacity of B-90 using the Box–Behnken design of experiment (DOE) methodology. Seventeen experiments were carried out, as shown in Table 8, which presents the experimental results and predicted values for each condition. The adsorption capacity as response factor varied in the range 24.67–423.15 mg/g and the following model equation was proposed:

$$Y = 124.886 + 17.346X_1 - 133.04X_2 + 74.339X_3 - 24.518X_1X_2 + 11.928X_1X_3 - 33.123X_2X_3 + 8.377X_1^2 + 91.248X_2^2 - 26.492X_3^2$$

Where Y is the predicted response value adsorption capacity and X_1, X_2, and X_3 are the values of the initial pH, dosage, and initial MB concentration, respectively.

Table 7 Microstructural properties of the biochars and adsorption capacity for MB

	B-0	B-50	B-70	B-90
S_{BET} (m^2/g)	10.8±1.9	511±12.0	435±23.3	433±7.5
V_{total} (cm^3/g)	0.015	0.24	0.22	0.21
V_{mic} (cm^3/g)	0.002	0.21	0.19	0.18
V_{meso} (cm^3/g)	0.013	0.03	0.03	0.03
AV[a] (nm)	5.7	1.9	2.0	1.9
Q_e[b] (mg/g)	17.48±1.13	156.62 ± 10.01	204.56 ± 5.58	420.86 ± 1.01
$Q_e/(S+O)/C$[c] (mg/g)	92	324.27	394.14	714.53
Q_{SA}[d] (mg/m^2)	1.62	0.30	0.47	0.97

[a]The average pore radius [b]MB adsorption capacity [c]The ratio of MB adsorption capacity to (S+O)/C molar ratio [d]Surface area-normalized MB adsorption capacity

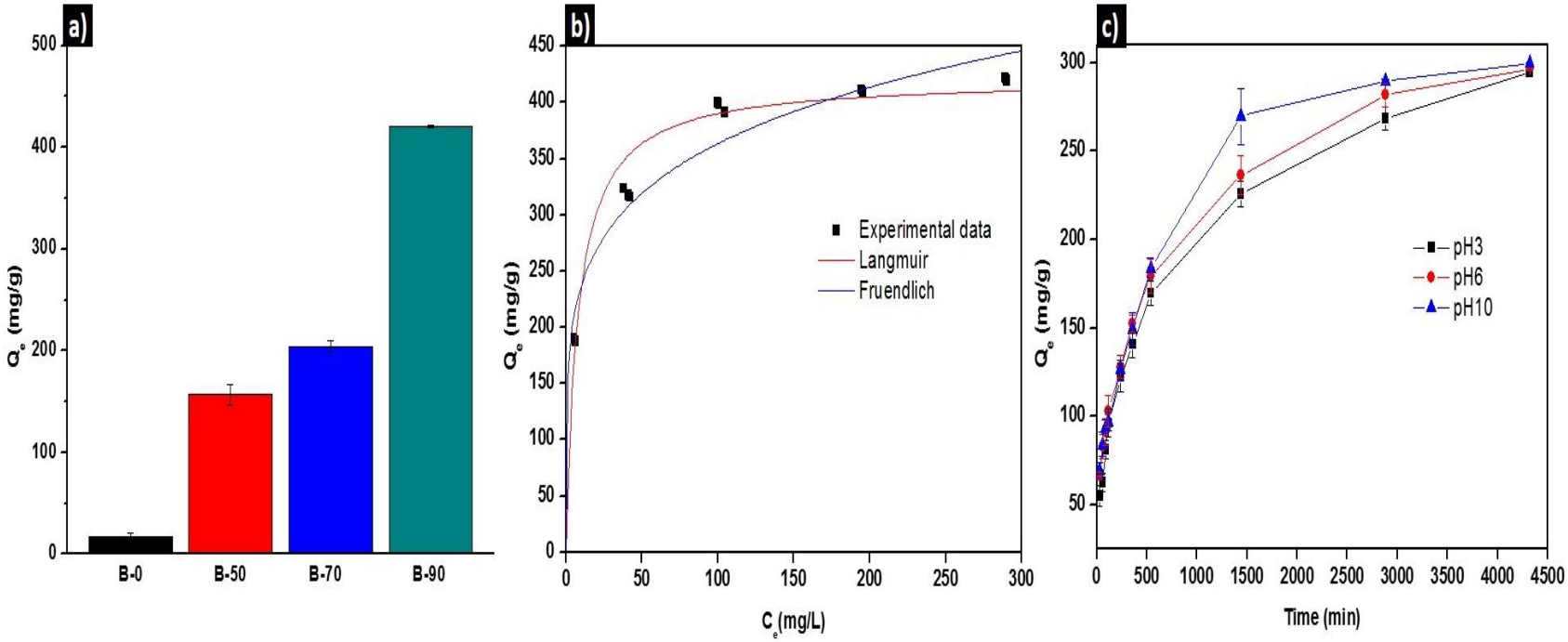

Figure 9. a) Adsorption capacity of B-0, B-50, B-70, and B-90 for MB, b) adsorption isotherm of B-90, and c) adsorption kinetic of B-90 at different pH condition

As shown in Table 9, the ANOVA of the quadratic regression model demonstrates the significance of the regression model with the Fisher F test (37.32) and Prob > F (0.0005)[77, 78]. The determination of coefficients (R^2) and adjusted R^2 (R_{adj}^2) were calculated to evaluate the fit of the model. The model with the high values for R^2 (0.9853) and R_{adj}^2 (0.9589), as shown in Table 9, indicated close agreement between the experimental results and the predicted adsorption capacity where 1% of the total variation was not explained by the model. t-values and p values were determined to confirm the significance of each coefficient in the model. Table 10 lists the t values and p values for each coefficient; a value of Prob > t less than 0.05 indicates that the model terms are significant in the model, while model terms higher than 0.05 are insignificant[78]. As shown in Table 10, the dosage of adsorbent was negatively significant on the adsorption capacity of B-90 for MB, whereas the initial MB concentration was positively significant for the adsorption capacity of B-90 on MB. The quadratic effect of the dosage of the adsorbent was also significant on the adsorption capacity. Table 10 indicates that there was no significant interaction effect among the model terms on the adsorption capacity. This means that the level of factors or the type of factors need to be changed for optimization. Compared to the other factors, the dosage of the adsorbent was the most significant factor because it had the lowest value for Prob > t.

Table 8 Box–Behnken experimental design

Variables	Factor code	Level of factor		
		-1	0	+1
pH	X1	2	6	10
Adsorbent dosage (mg)	X2	10	45	80
Initial concentration (mg/L)	X3	100	300	500

	Coded variables			Adsorption capacity (mg/g)		
Run	X1	X2	X3	Actual data	Predicted data	Residual
1	0	+1	+1	124.24 ± 1.00	97.82	26.42
2	0	-1	+1	420.86 ± 1.00	430.14	-9.28
3	-1	-1	0	327.66 ± 10.22	315.69	11.97
4	-1	0	0	41.46 ± 2.17	27.01	14.45
5	+1	+1	0	72.33 ± 2.44	84.30	-11.97
6	0	0	0	122.09 ± 7.06	124.89	-2.8
7	0	0	0	128.13 ± 5.14	124.89	3.24
8	+1	0	+1	195.94 ± 4.40	210.38	-14.44
9	-1	+1	0	74.91 ± 0.03	98.64	-23.73
10	0	0	0	124.44 ± 2.79	124.89	-0.45
11	+1	-1	0	423.15 ± 1.91	399.42	23.73
12	-1	0	+1	149.15 ± 9.71	151.84	-2.69
13	0	-1	-1	188.80 ± 1.00	215.22	-26.42
14	+1	0	-1	40.54 ± 3.20	37.85	2.69
15	0	+1	-1	24.67 ± 0.41	15.39	9.28

Table 9 Analysis of variance (ANOVA) for a quadratic model and a summary of fit

ANOVA					
	Degrees of Freedom	Sum of Squares	Mean Square	F Ratio	Prob > F
Model	9	230543.16	25615.9	37.3226	0.0005
Error	5	3431.69	686.3		
C. Total	14	233974.85			
Lack of Fit	3	3413.1830	1137.73	122.9663	0.0081
Pure Error	2	18.5047	9.25		
Total Error	5	3431.6877			

Summary of Fit	
RSquare	0.9853
RSquare Adj	0.9589
Root Mean Square Error	26.20
Mean of Response	163.9
Observations (or Sum Wgts)	15

Table 10 Significance of regression coefficients

Term	Estimates	Std Error	t Ratio	Prob > t
Intercept	124.89	15.13	8.26	0.0004
X_1	17.35	9.26	1.87	0.1200
X_2	-133.04	9.26	-14.36	< 0.0001
X_3	74.34	9.26	8.03	0.0005
X_1X_2	-24.52	13.10	-1.87	0.1201
X_1X_3	11.93	13.10	0.91	0.4043
X_2X_3	-33.12	13.10	-2.53	0.0526
X_1^2	8.38	13.63	0.61	0.5658
X_2^2	91.25	13.63	6.69	0.0011
X_3^2	-26.49	13.63	-1.94	0.1096

3.3.4 Adsorption isotherm model

In this study, Langmuir and Freundlich isotherm equations in nonlinear form were fitted to the equilibrium data of the MB adsorption of adsorbents to determine how MB was distributed on the surface of biochar in the equilibrium state. Langmuir isotherm model is for describing monolayer adsorption with the surface homogeneity of the adsorbents, while, Freundlich isotherm model is for non-ideal reversible and multilayer adsorption process with non-uniform distribution of affinity on the heterogeneous surface[73, 79]. Table 11 shows the isotherm parameter and coefficient of determination (R^2)

for each model equation and Figure 9b) shows the corresponding fitting curves on the equilibrium data. The Langmuir isotherm model had a higher R^2 (0.9607) than the Freundlich isotherm model (0.9410), which means that the surface of the biochar was a homogeneous surface that contained identical and equivalent active sites attracting MB[69, 73]. Furthermore, it indicates that favorable adsorption behavior was monolayer adsorption including physical and chemical adsorption supported by a plateau, as shown in Figure 9b). The maximum adsorption capacity obtained via Langmuir adsorption was 421.18 mg/g, which is superior and comparable to the values of other adsorbents reported in the literature. Dimensionless separation factor (R_L)[80], which is an important characteristic of Langmuir isotherm, can be represented as:

$$R_L = \frac{1}{1 + K_L C_0}$$

where K_L (L/mg) is the Langmuir constant and C_0 is the initial concentration (mg/L). The value of R_L indicates the adsorption nature as irreversible (R_L=0), favorable (0< R_L<1), linear (R_L=1) and unfavorable (R_L>1)[80]. The value of R_L for MB adsorption on B-90 was between 0.016 and 0.074, which means that the adsorption for MB on B-90 was a favorable process.

Table 11. Langmuir and Freundlich constants

Dyes	Biochar	Langmuir constants			Freundlich constants		
		Q_m (mg/g)	K (L/mg)	R^2	K_F (L/mg)	1/n	R^2
MB	B-100	421.18	0.13	0.9607	153.68	0.19	0.9410
MO	B-100	217.02	0.020	0.9464	30.24	0.32	0.9313

3.3.5 Adsorption kinetics

Kinetic experiments were conducted at different pH conditions of 3, 6, and 10. According to Figure 9c), the adsorption rate and adsorption capacity increased as the pH condition was increased from 3 to 10. The surface of B-90 probably became more negative as pH increased by the deprotonation of surface functional groups[68]. The increase of electric interactions between the positively charged MB and the negatively charged surface of the adsorbents facilitated the adsorption, resulting in increasing the adsorption rate and capacity. This observation corresponds to previous reports[68, 69, 81].

Four different adsorption kinetic models, a pseudo-first order, pseudo-second order, Nth order model, and intra-particle diffusion models, were applied to fit each experiment data under different pH conditions to determine the adsorption mechanism that controlled the adsorption process. The corresponding fitting curves are shown in Figure 10a), b), and c), while the kinetic parameters are in Table 12. The R^2 value from Nth order model was the highest, followed by the intra-particle diffusion, pseudo-second order, and then pseudo-first order for all pH conditions; this means that the Nth order model was the most suitable for describing the kinetics of the adsorption of MB on adsorbents compared

to the other models, regardless of pH condition indicating that pH had a negligible effect on the adsorption mechanism.

Figure 11 shows two separate linear regions for the adsorption of MB on B-90 according to the intra-diffusion model. For pH 3 and 6, the first region was 0.7–3 $min^{1/2}$, while the first region was 0.7–4.9 $min^{1/2}$ for pH 10. Both first regions represented the stage of film diffusion[69]; the longer range of the first region for pH 10 is probably due to the higher degree of adsorption sites for B-90 in pH 10 compared to in pH 3 or 6. The second stage (the 3–8.5 $min^{1/2}$ range for pH 3 and pH6 and the 4.9–8.5 $min^{1/2}$ range for pH 10) represents the intraparticle diffusion[69]. The kinetic constants for first region (K_{i1}) are larger than the kinetic constants for the second region (K_{i2}) regardless of the pH. Even though intraparticle diffusion is a slow process, the plot does not pass through the origin; this means that the intraparticle diffusion was not a rate determined mechanism and the film diffusion effect is not negligible for the adsorption of MB on B-90[69, 77].

Table 12 Kinetic constants for kinetic models

pH condition	Model	Parameter 1	Parameter 2	R^2
3	First-order	k_1: 0.00254	Q_e: 262.33	0.9036
6		k_1: 0.00288	Q_e: 267.38	0.8694
9		k_1: 0.00259	Q_e: 283.62	0.8934
3	Second-order	k_2: 1.09×10^{-5}	Q_e: 293.66	0.9574
6		k_2: 1.31×10^{-5}	Q_e: 294.90	0.9381
9		k_2: 1.11×10^{-5}	Q_e: 312.58	0.9400
3	Nth-order	k_3: 7.49×10^{-8}	Q_e: 333.31	0.9902
6		k_3: 1.07×10^{-7}	Q_e: 329.01	0.9855
9		k_3: 7.63×10^{-8}	Q_e: 350.51	0.9840
3	Intra-particle	k_i: 4.04	C: 51.22	0.9610
6		k_i: 3.95	C: 63.47	0.9579
9		k_i: 4.15	C: 63.20	0.9309

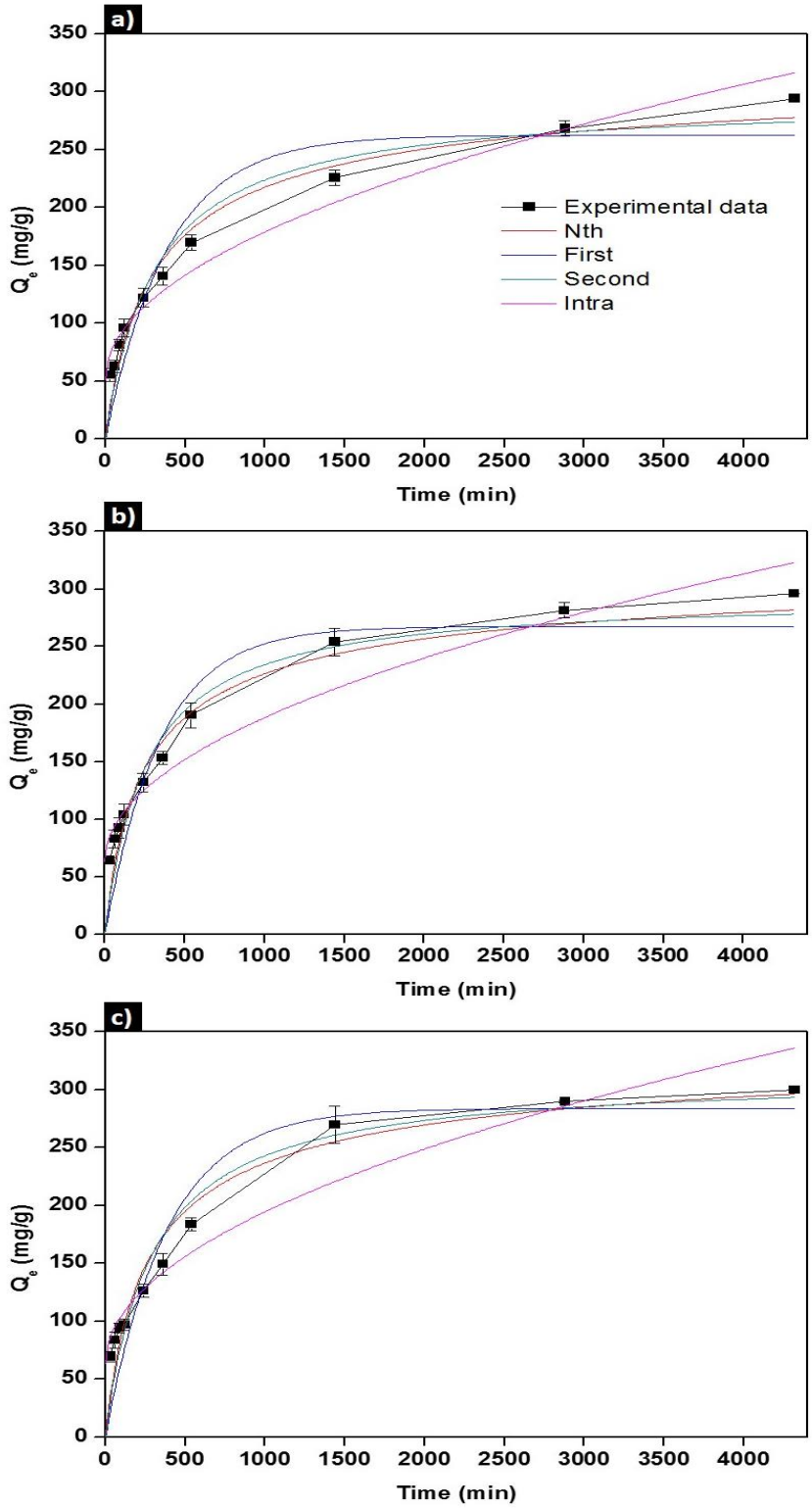

Figure 10. Effect of contact time on the adsorption of MB on B-90 at a) pH3, b) pH6, and c) pH10

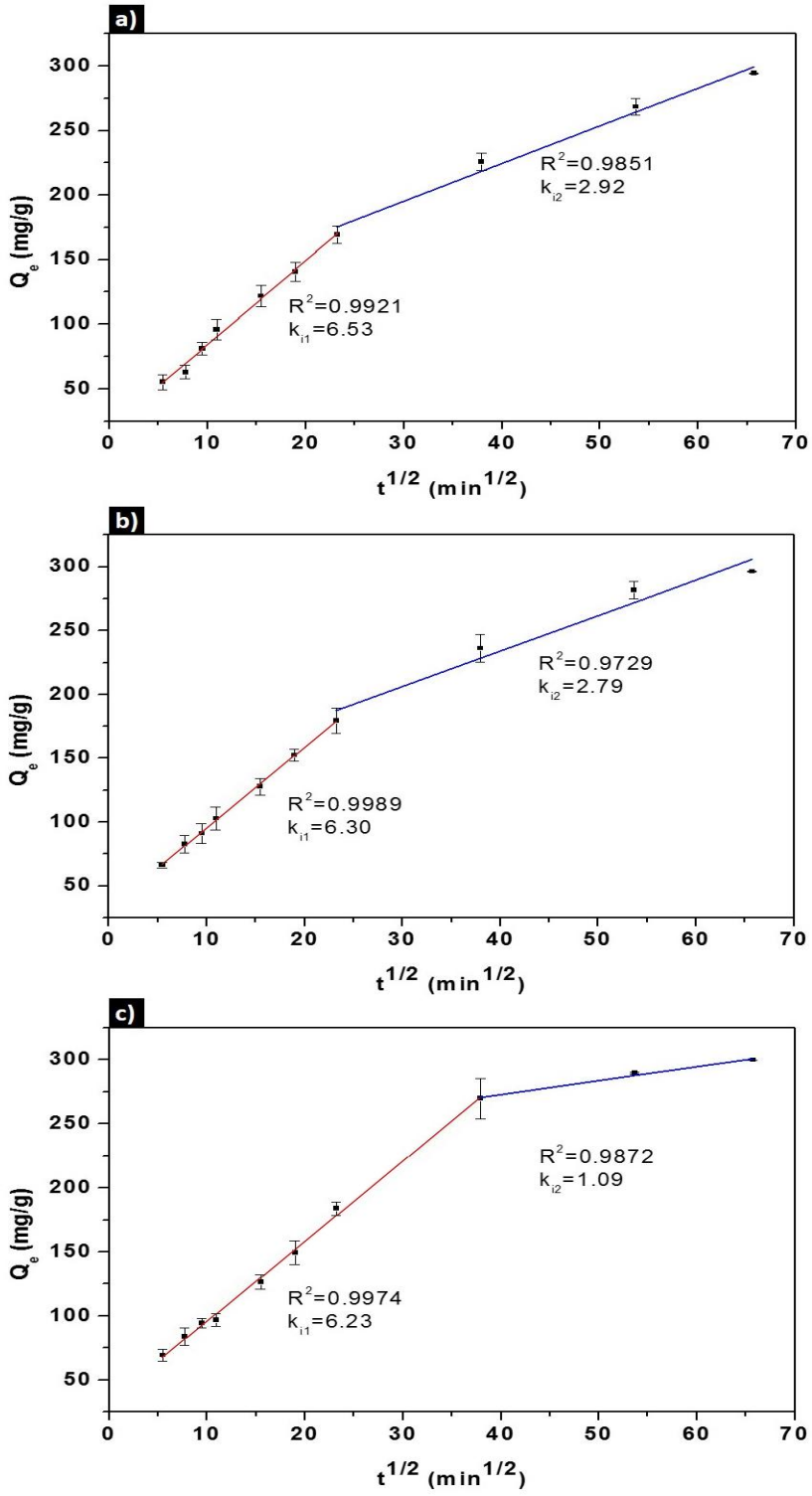

Figure 11. Intraparticle diffusion kinetic plots for the adsorption at a) pH3, b) pH6, and c) pH10

3.3.6 Binary system adsorption

Adsorption tests were performed on mixtures of MB and MO to confirm the effect of competitors on the adsorption capacity of MB in a binary system. The ratios of MB to MO in the mixtures were 5:1, 2:1, 1:1, and 1:2. As shown in Figure 12a), we observed the lower value of the adsorption capacity compared to the adsorption capacity for MB in a single system. The adsorption capacity decreased from 5:1 to 1:1; however, the adsorption capacity increased at 1:2 but was still a lower value than in the single system. This observation indicates that MO negatively affected the adsorption capacity of MB on the adsorbent. Adsorption tests of B-90 on a single MO solution at 50 ppm, 125 ppm, 250 ppm, and 500 ppm under the same experimental conditions was performed to check the effects of 250 ppm MB on the adsorption capacity of MO. As shown in Figure 12b), 250 ppm of MB negatively affected the adsorption capacity of MO on adsorbents at initial concentration from 50 ppm to 250 ppm. Interestingly, the adsorption capacity of adsorbents at 500 ppm MO with 250 ppm MB was higher than the value obtained from the single component test; this might be due to interactions between MB and MO. This observation implies that BC90 has a higher selectivity for MB than MO when MO is at a low concentration; this means that B-90 can be used to separate a single dye chemical from a mixture of MB and MO within a certain ratio.

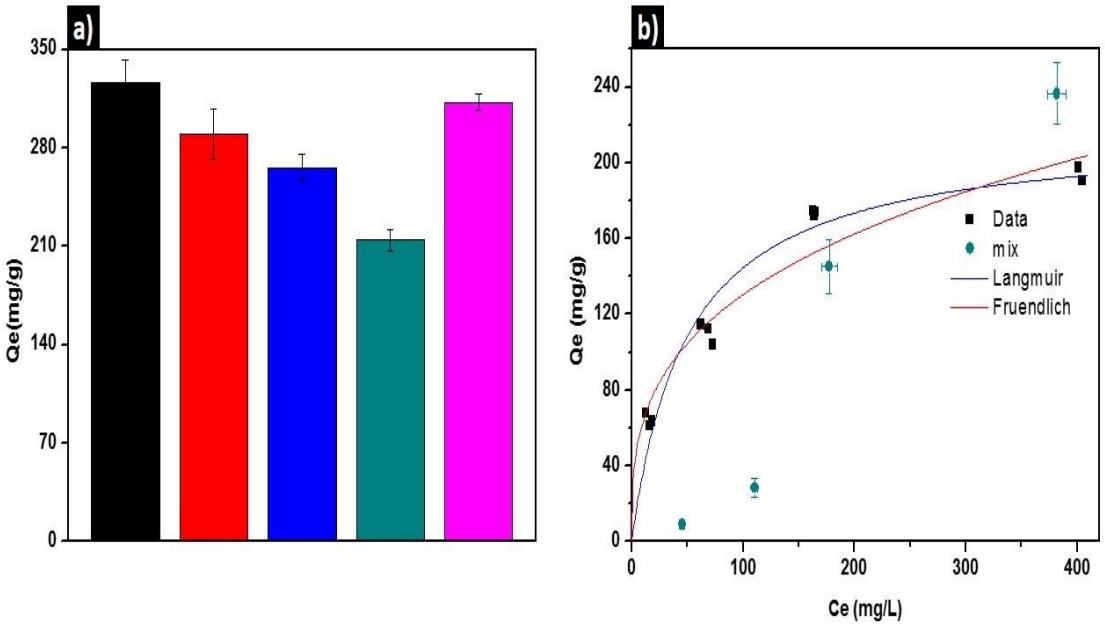

Figure 12. a) adsorption capacity of B-90 for MB in binary system and b) adsorption isotherm of B-90 for MO in single system and binary system

3.4 Conclusions

Surface functionalized biochar was produced by sulfuric acid treatment under various conditions for the removal of MB. Sulfuric acid was significantly helpful for improving the adsorption capacity of MB on biochar by introducing surface functional groups and microporosity. The adsorption capacity of MB on acid-treated biochar increased 200-fold compared to untreated biochar. Adsorption isotherms and kinetic studies revealed that electrical interaction was a crucial factor in the adsorption. The Langmuir isotherm was fit the data well and the adsorption kinetic of MB on the sample followed Nth order kinetics. The binary system adsorption experiment revealed that acid-treated biochar had higher adsorption selectivity on MB than methyl orange. Therefore,

the functionalized biochar with high adsorption capacity and selectivity on MB can be used to separate MB from the dye mixtures produced from textiles and dyeing industry. Furthermore, the sulfonated groups on biochar samples mean that prepared biochar samples can be used as solid acid catalysts for the esterification reaction.

CHAPTER IV

SELECTIVE PRODUCTION OF HIGH VALUE-ADDED PRODUCTS BY VACUUM PYROLYSIS OF ASHE JUNIPER WASTE TREATED WITH METAL SALTS AND MICROWAVE-ASSISTED PRETREATMENT

4.1 Introduction

Pyrolysis is a thermochemical process to decompose organic compounds, such as biomass, at elevated temperatures in the absence of oxygen. Using pyrolysis, biomass can be converted to syngas, bio-oil and biochar[43]. Syngas and bio-oil are considered major intermediate products that can be used to create alternatives to conventional fuels[43].

Bio-oil is composed of hundreds of chemicals, including some high value added chemicals, e.g. levoglucosenone (LGO)[28], which can be recovered by separation processes such as distillation. For example, LGO can be used as a building block[29, 30] for pharmaceutical synthesis, such as (+)-chloriolide (antibiotic) and ras proteins activation inhibitors (anticancer drug); 1,6-hexanediol, widely used for polyester, polyamide, and polyurethane production; and 5-hydroxymethyldihydrofuranone (5-HMF), used for pharmaceuticals, fuels, and nucleic acids. Therefore, bio-oil is an excellent raw source to obtain specific value-added chemicals.

However, recovery of these high value-added chemicals from bio-oils is technically challenging and generally uneconomical due to the compositional complexity and low concentration of each component in bio-oil. Therefore, production rate and

selectivity for the required chemicals must be improved for successful commercialization. Catalytic selective pyrolysis is one method to produce high value-added chemicals with high production rate and selectivity from biomass.

Levoglucosenone is rarely produced by pyrolysis[28], and several catalytic pyrolysis methods have been proposed to increase LGO production rate and selectivity. Dobele et al. conducted catalytic pyrolysis with phosphoric acid-impregnated cellulose and biomass, producing maximum selectivity of 30%[32, 33]. Dobele et al. also investigated the effect of Fe^{3+} on the yield of LGO, of which maximum yield was 25.7%, derived from cellulose[34]. Branca et al. investigated acid-catalyzed pyrolysis of concorbs, producing 4.6% yield of LGO[35]. Solid acids such as sulfated ZrO2, sulfated TiO2, and sulfated TiO2/Fe2O3 were explored to improve LGO yield based on cellulose to 7.25%[36], 5.69%[36], and 15.4%[37], respectively. Xin et al. reported LGO selectivity up to 82.6% from cellulose impregnated with phosphoric acid using an evaporation method[28], and also showed that sulfates could increase LGO yield significantly.

Metal salts and metal cation effects on LGO yield and selectivity has been rarely investigated. Particularly, the role of metal cations on LGO yield and selectivity should be confirmed by comparison between the effects from different metal sulfates. Therefore, the current study contributes the conversion of biomass waste used for remediation of contaminated soils, which is probably contaminated with metal salts, into high value-added products

Most research regarding the production of high value-added chemicals was conducted with cellulose rather than raw biomass, which consists of cellulose,

hemicellulose, and lignin. Zheng et al. reported that lignin content affected the yield of levoglucosan[82]. Similarly, we think that the lignin content in biomass might also affect the yield and selectivity of LGO, because dehydration of levoglucosan is one possible pathway to LGO during pyrolysis[83-85]. Therefore, the effect of biomass chemical composition, such as lignin content, on the selectivity and yield of compounds in bio-oil should be investigated.

Microwave-assisted organosolv treatment (MSOT) is an efficient way to alter the chemical composition of biomass[82, 86, 87]. In this research, we applied MSOT using different solvents to investigate the effects on yield and composition of bio-oil.

Ashe Juniper is a native and rapidly expanded specie influencing production, composition, and structure of rangeland plant communities and hydrology of many areas. Management for Ashe Juniper clearing using the hydraulic shears or a bulldozer might produce large quantities of waste[40]. However, Ashe juniper waste has high carbon content and could be used as a renewable carbon source to produce high value added chemicals alternatives to fossil fuel derived chemicals. Therefore, the main objective of this research is to improve LGO production yield and selectivity by catalytic vacuum pyrolysis and alteration of the chemical composition of Ashe Juniper waste. The specific objectives are as follows.

a. Evaluate the effect of process parameters on yield and composition of products by vacuum pyrolysis.
b. Investigate the effect of metal salt type and concentration on yield and selectivity of compounds in bio-oil.

c. Determine the effect of metal cations on yield and selectivity of LGO.
d. Investigate the effect of microwave-assisted treatment on the chemical composition of biomass and bio-oil.

4.2 Materials and methods

4.2.1 Feed material

Ashe juniper waste was crushed by a wilye mill using a 2 mm screen and stored in a zip-lock bag at a room temperature. The samples were dried for two hours before pyrolysis. The volatility and fixed carbon and ash contents were determined following ASTM D3172. The elemental composition was determined with an ultimate analyzer (a Vario MICRO elemental analyzer).

4.2.2 Microwave-assisted solvothermal treatment of Ashe juniper waste

Two different solvent mixtures, ethanol, acetic acid, and water with and without sulfuric acid (50:50:50 v/v/v, 0.1M H_2SO_4), were prepared, respectively. Ashe juniper waste was mixed with each mixture at 1:10 solid:liquid ratio (w/v) in a borosilicate round bottom glass flask. The mixture was solvothermally treated in a microwave oven at 350W for 10 min. A condenser with 10°C water was installed for reflux. After the reaction, the mixture was filtered to collect insoluble residues. Insoluble residues were washed three times using deionized (DI) water and dried in an oven at 60°C for 24 h.

4.2.3 Metal salts impregnation

Each 60 ml of 0.1, 0.2, and 0.4 M solution of $ZnSO_4$, $CuSO_4$, and NaCl, respectively, were prepared in DI water. 10 g of Ashe juniper was submerged in each solution. The mixtures were individually mixed on a rotary shaker at 200 rpm for 24 h. Then, the mixture was evaporated in the oven at 105°C for 24 h.

4.2.4 Vacuum pyrolysis for the production of oils

Ashe juniper was pyrolyzed in a homemade vacuum pyrolysis machine, as shown in Figure 13. To investigate the effect of temperature and vacuum pressure on product yield and composition, 10 g of Ashe juniper waste was placed in a glass flask (Chemglass) inserted into an electrical furnace. The flask was connected to a condenser to collect the relatively heavy bio-oil (Fraction 1). The condenser was connected to a subsequent cold trap to collect the relatively light bio-oil (Fraction 2). The cold trap was connected to a mechanical vacuum pump. The system was evacuated at 0.09, 0.7, and 3 kPa (denoted as 1, 2, and 3, respectively). The reactor was heated to 350, 450, and 520°C for each pressure with a heating rate of 20°C/min controlled by PID controllers. Each pyrolysis condition is denoted as temperature-pressure. For example, 350-1 means that the biomass was pyrolyzed at 350°C and 0.09 kPa. The system was maintained at the final temperature, for 1 h, and then Fraction 1 and Fraction 2, and biochar were collected.

The yield of each sample was calculated by weighing the various remainders after the vacuum pyrolysis. The total oil yields were calculated by summing Fraction 1 and Fraction 2 yields. Biochar produced at certain temperature and pressure was named B-

temperature-pressure. For example, B-350-1 refers to biochar produced at 350°C and 0.09 kPa. As a control, biochar was produced at 520°C and atmospheric nitrogen pressure. Each run was conducted 3 times.

To test the effects of metal impregnation and microwave-solvothermal treatment, 10 g of prepared samples were pyrolyzed at 0.7 kPa and 450°C. Biochar and Oil were collected and yields were calculated as described above.

4.2.5 Oils analysis

Chemical compositions of Fraction1 and Fraction 2 were measured using GC-MS (A Shimadzu QP2010Plus) using helium as a carrier gas, and ZB5MS GC-MS (30 m × 0.25 mm × 0.25 μm thick) column. The column temperature program was set as follows: an injection temperature of 295°C; a column oven temperature of 45°C at the beginning and held for 5 min, then ramped to 330°C at the rate of 5°C/min and held for 5 min; a MS ion source temperature of 250°C, and an interface temperature of 320°C.

$$\text{Relative selectivity } (\%) = \frac{\text{Specific peak area}}{\text{Total peak area}} \times 100$$

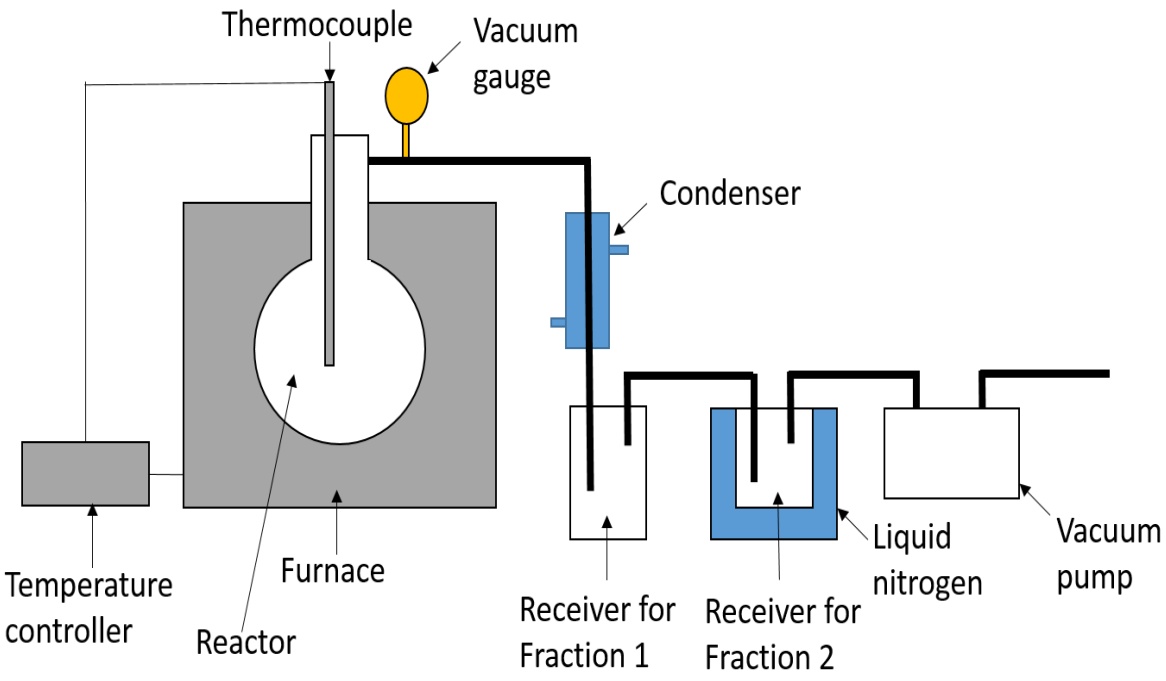

Figure 13. Vacuum pyrolysis experimental setup

4.3 Results and discussion

4.3.1 Temperature and vacuum pressure effects on product yields and compositions

This work examined the effect of pyrolysis temperature and vacuum pressure on product yields. As shown in Figure 14, pyrolysis temperature significantly affected bio-oil and biochar yields. Total bio-oil yield increased from 35.9% to 55%, and biochar yield decreased from 39% to 15.8% with increasing pyrolysis temperature. This was attributed to increased organic vapor removal from the biomass under increased pyrolysis temperature. In particular, the yield of Fraction 1, consisting of heavy molecular weight materials, was linearly correlated with the system temperature. However, the highest yield of Fraction 2 consisting of light molecular weight materials was obtained at 450 °C due to secondary decomposition for higher temperatures.

For constant temperature, varying the vacuum pressure of the system significantly affected the product yields. The lower vacuum pressure increased the yield of Fraction 2 because the relatively lightweight volatiles could be more easily diffused further due to increased mean free path under the lower pressure. In contrast, char yield decreased as pressure decreased, probably due to easier volatile escape from the biomass. Lower vacuum pressure also increased total oil and Fraction 1 yields at 350°C, but, the system pressure had only minor effect on yields of total bio-oil at 450°C and 520°C. However, Fraction 1 yields decreased at 450°C and 520°C for decreased vacuum pressure due to two possible reasons: a greater amount of relatively lighter vapor was diffused to Fraction 2 under lower vacuum pressure; and bio-oil loss may affect the yield of Fraction 2 as more

vapor condensed in the line between the receiver and cold trap, due to the increased mean free path at the relatively higher pyrolysis temperature and lower vacuum pressure.

Table 13 shows some valuable chemicals that were identified in Fraction 1 and Fraction 2. Average boiling point of chemicals identified in Fraction 2 was approximately 140°C, and of Fraction 1 was 220°C. Fraction 2 was largely composed of acetol, 2-methoxy-N-methylethylamine, ethyl pyruvate, methyl pyruvate, FF, and levoglucosan. Acetol is widely used as a precursor in the chemical industry, and as a fragrance in the food industry[88]; methyl pyruvate can be used as a precursor to synthesize terephthalic acid as a precursor to the polyester[49]; ethyl pyruvate is used as a flavoring agent[89]; FF is an important renewable chemical for producing furan, tetrahydrofuran, and resins[90]; and levoglucosan can be used for biochemical processes[91]. Fraction 2 was mainly composed of cedrol oils, such as cedren, thujopsene, and cedol, which are used in the perfume industry[92].

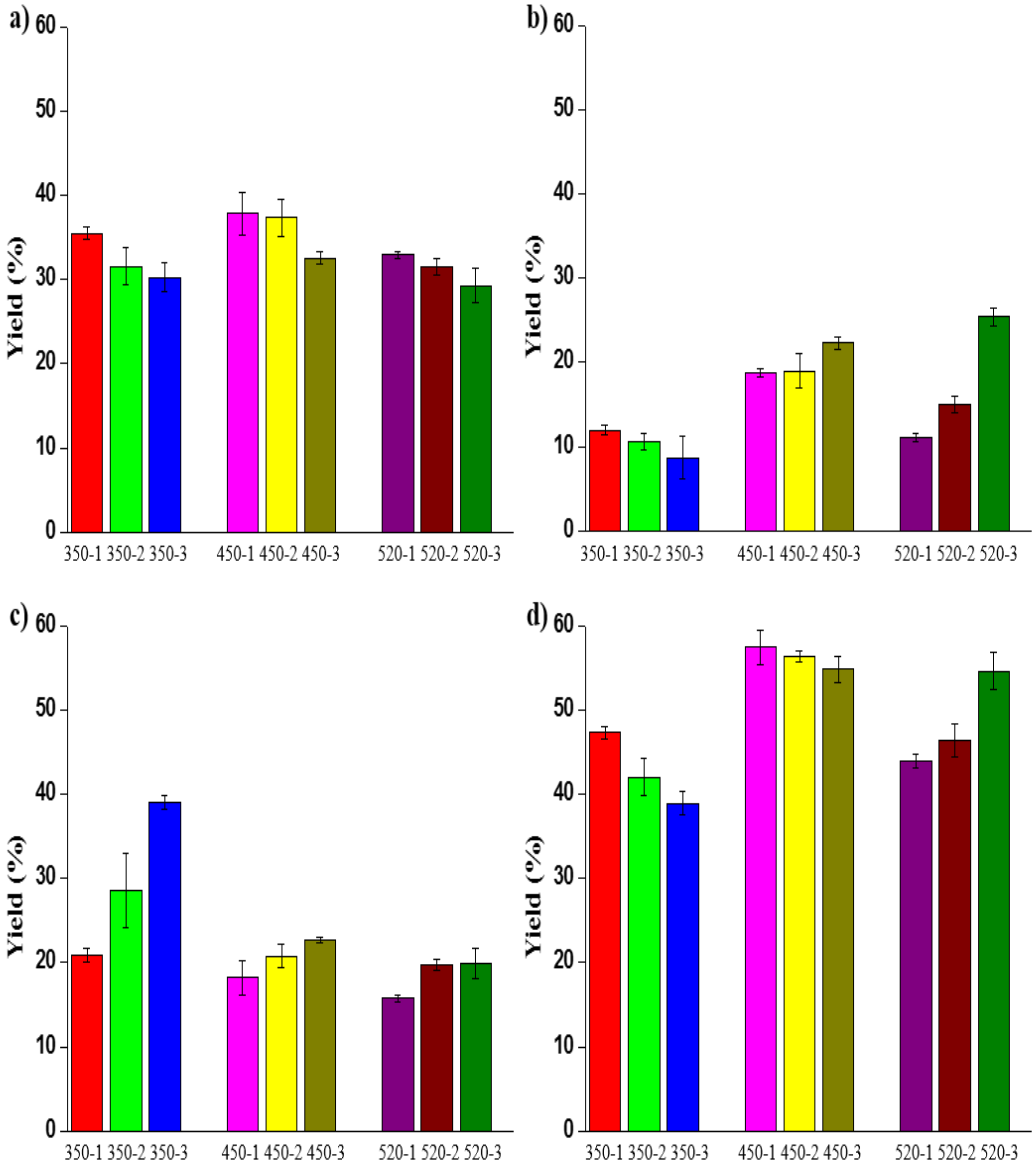

Figure 14. Yield of a) Fraction 2, b) Fraction 1, c) Biochar yield and d) Total oil under different pyrolysis conditions

Table 13 The main chemicals in Fraction 1 and Fraction 2

Fraction 1	Relative selectivity (%)								
Compounds	350-1	350-2	350-3	450-1	450-2	450-3	520-1	520-2	520-3
Acetol	27.21	22.97	19.63	23.32	19.01	25.46	24.74	22.6	25.66
2-Methoxy-N-methylethylamine	6.74	8.49	3.56	8.37	10.28	2.99	11.69	6.97	5.77
Ethyl pyruvate	8.66	8.08	5.11	10.76	5.67	4.75	9.3	7.17	6.19
Methyl pyruvate	11.19	10.78	4.76	11.28	12.17	7.7	10.94	8.2	8.7
Furfural	4.54	4.88	4.59	4.22	4.42	4.6	4.52	4.39	4.29
Levoglucosan	7.58	10.49	13.14	6.84	5.91	7.49	6.71	7.74	5.1
Fraction 2	Relative selectivity (%)								
Compounds	350-1	350-2	350-3	450-1	450-2	450-3	520-1	520-2	520-3
Cedren	3.96	11.5	23.53	4.93	3.51	7.21	12.15	3.55	5.45
Thjopsene	3.39	6.35	9.01	2.5	1.75	2.76	1.77	1.76	1.48
Cedrol	19.19	38.12	17.87	30.85	17.34	12.65	30.51	39.93	11.04

4.3.2 Metal salts impregnation effects on product yield

Figure 15 shows the yields of products derived from each sample. Different metal salts affected product (biochar, Fraction 1 and Fraction 2) yields differently. Metal salt impregnation increased the yield of biochar compared to the yield without impregnation, with maximum biochar yield obtained from sodium chloride impregnated samples. This result is consistent with previous studies that have shown that metal cations promoted the formation of biochar[13, 53].

Maximum Fraction 2 yield was obtained from pyrolysis of $ZnSO_4$-impregnated samples, while, lower yields from $CuSO_4$ and NaCl impregnated samples, respectively. In contrast, Fraction 1 yield obtained from the metal salts impregnated samples were lower than from non-impregnated sample. This observation was opposite to the trend shown in biochar production that the yield obtained from the impregnated sample was higher than the non-impregnated sample. These trends were strongly related to various effects of metal salts on the heavyweight molecules, such as pyrolytic lignin, which is a major component of Fraction 1. Metal salts can decompose heavyweight molecules into lightweight molecules or non-condensable gases[13] resulting in decreased yield of Fraction 1, but increased yield of Fraction 2 as observed for $ZnSO_4$-impregnated samples. Metal salts can also catalyze heavyweight molecule polymerization during pyrolysis[13], resulting in increased biochar yield, as observed for impregnated samples. Therefore, selection of metal salt is important to control product yield.

Biochar samples can be used for several applications. Pyrolysis of metal salt impregnated samples is an efficient method to produce functionalized biochar suitable for adsorbents and catalysts[8]. These biochar samples contain high concentrations of certain metal elements, which can be regenerated by burning the biochar and employing as nutrient in fertilizer and synthesis of catalysts[7, 10].

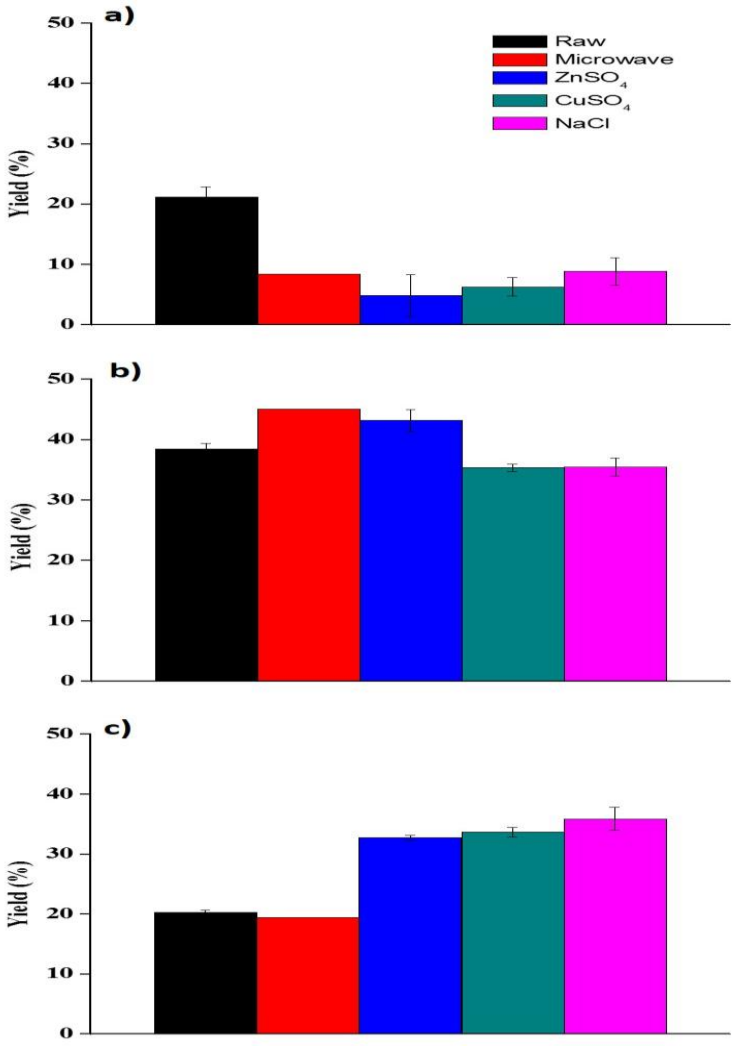

Figure 15. Yield of a) Fraction 1, b) Fraction 2, and c) Biochar

4.3.3 Metal salt impregnation effects on the chemical composition of Fraction 2

Table 14 shows that the major identified products within Fraction 2 for the various treatments. FF and LGO were the major compounds for $ZnSO_4$ and $CuSO_4$ impregnated samples, and Glycoaldehyde dimethyl acetal, phenolic compounds, and 1,2-Cyclopentanedione were the major compounds derived from NaCl impregnated samples. Figure 16 shows that each Fraction 2 sample had different peak positions in ion chromatograms, which indicates the effect of impregnation on the change of chemical composition. Differences for major compounds were significant. Thus, metal salts are crucial factors to modify the selectivity of the target chemical, which is consistent with previous reports[93-95]. It is known that sulfate ions have a catalytic effect converting cellulose and hemicellulose into LGO and FF[28, 30, 96]; sulfate ions in $ZnSO_4$ and $CuSO_4$ probably catalyzed the conversion of cellulose and hemicellulose in Ashe juniper to LGO and FF; and zinc and copper ions presumably affect LGO and FF production differently.

To prove these assumptions, Ashe juniper impregnated with different concentrations of $ZnSO_4$ and $CuSO_4$ by evaporation methods were pyrolyzed under the same condition. Results are presented in the following sections.

Table 14 The main chemicals in Fraction 2

Fraction 1	**Relative selectivity (%)**		
Compounds	$CuSO_4$	$ZnSO_4$	NaCl
Aldehyde			
Glycolaldehyde dimethyl acetal	5.45	5.38	10.37
Esters			
1,2-cyclopentanedione	0	0	8.13
Acetic acid, dimethoxy-, methyl ester	0	0	3.7
Cyclopentanone	0	0	2.5
Pentanoic acid, 4-oxo-, methyl ester	1.97	0	0
Furan			
Furfural	15.92	9.97	0
Levoglucosenone	19.9	14.7	0
Sugars			
1,4:3,6-Dianhydro alpha.-d-glucopyranose	5.95	5.14	0
1,6-Anhydro-.beta.-d-talopyranose	0	0	1.63
2,3-Anhydro-d-mannosan	0	0	0.85
Levoglucosan	2.71	2.71	3.66
D-Allose	0	13.4	
Phenolic compounds	4.22	2.11	12.76

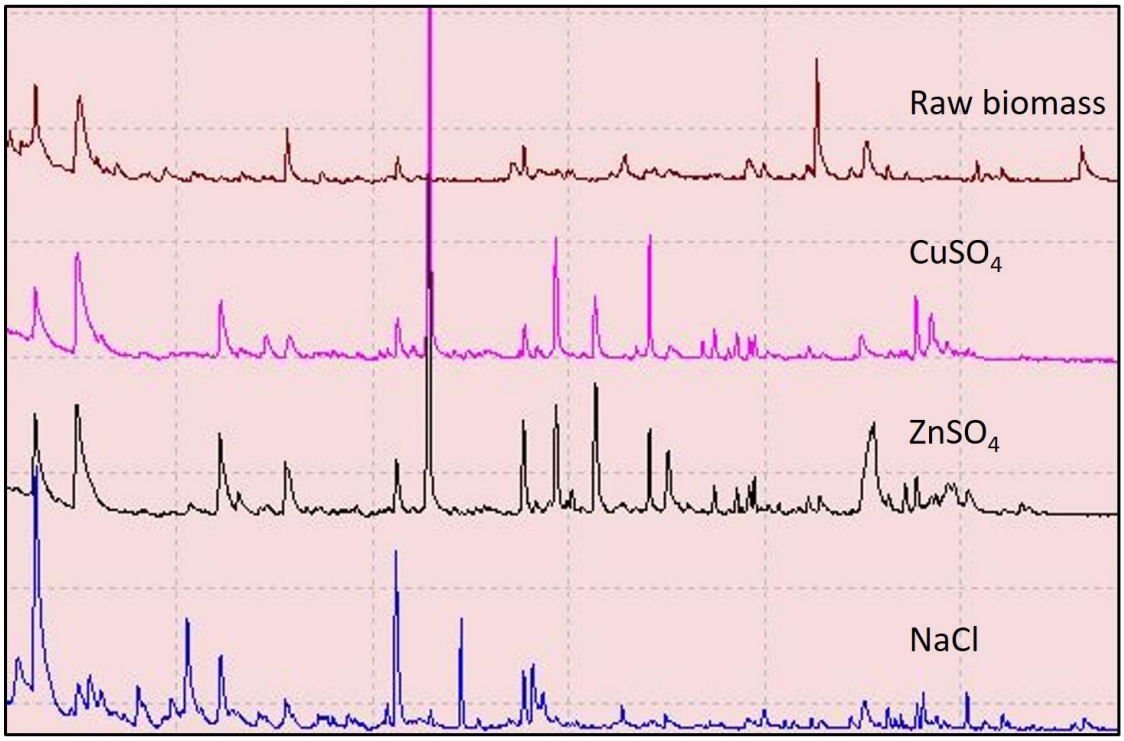

Figure 16. Ion chromatocrams of Fraction 2

4.3.4 Metal sulfate concentration effects on production yield

Figure 17 shows that concentrations of different metal salts affected the yield of product differently. For $ZnSO_4$ (Figure. 17a)), the yield of biochar increased, Fraction 1 decreased, and Fraction 2 did not change significantly with increasing $ZnSO_4$ concentration. As shown in Figure. 17b), the concentration of $CuSO_4$ shows similar effects on the yield of products as $ZnSO_4$. However, yields for biochar and Fraction 2 for $CuSO_4$ are lower than $ZnSO_4$ impregnated samples. This indicates that $ZnSO_4$ catalyzed the secondary decomposition reaction and repolymerization to a greater extent than $CuSO_4$.

For the experiment, the same moles of $ZnSO_4$ and $CuSO_4$ were impregnated into Ashe juniper waste. Therefore, cation type is an important factor to control the yield of the products if the same concentration of sulfate are used.

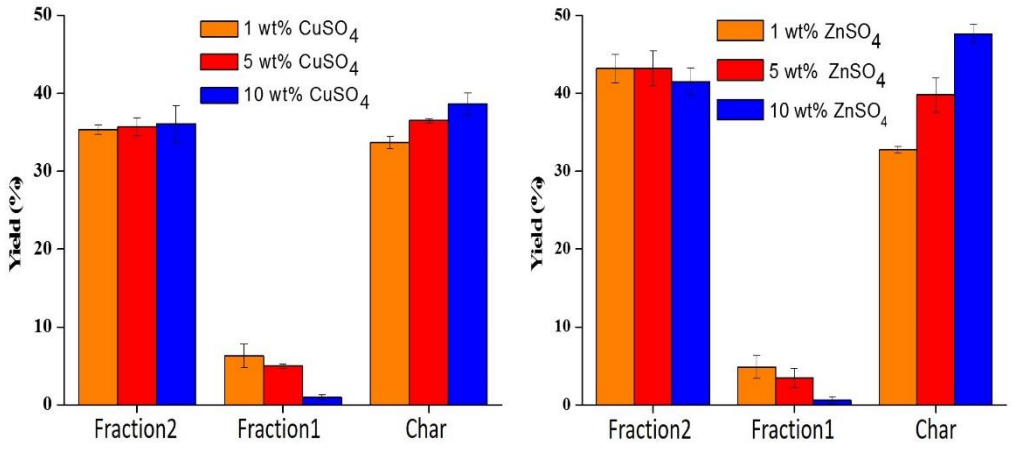

Figure 17. Yield of products derived from a) $CuSO_4$ treated sample and b) $ZnSO_4$

4.3.5 $CuSO_4$ and $ZnSO_4$ concentration effects on selectivity of furfural and levoglucosenone production

Figure 18 shows ion chromatograms for Fraction 2 from each sample. Peak positions are consistent, indicating that $ZnSO_4$ and $CuSO_4$ concentration did not affect chemical composition. However, the peak intensities for FF and LGO increased with

increasing concentration of both catalysts. Thus, it was confirmed that the concentration of catalysts affected the reaction rate, but did not change the reaction pathway. Figure 19 shows that LGO selectivity increased from 22.0% to 25.2% with increasing $CuSO_4$ concentrations four fold, and 15.0% to 27.2% for four fold increased $ZnSO_4$ concentration. While selectivity of FF increased from 15.4% to 18.73% as the concentration of $CuSO_4$ increased, and from 19.6% to 25.8% with increasing $ZnSO_4$. These results indicate that $ZnSO_4$ had more significant effects on selectivity than $CuSO_4$.

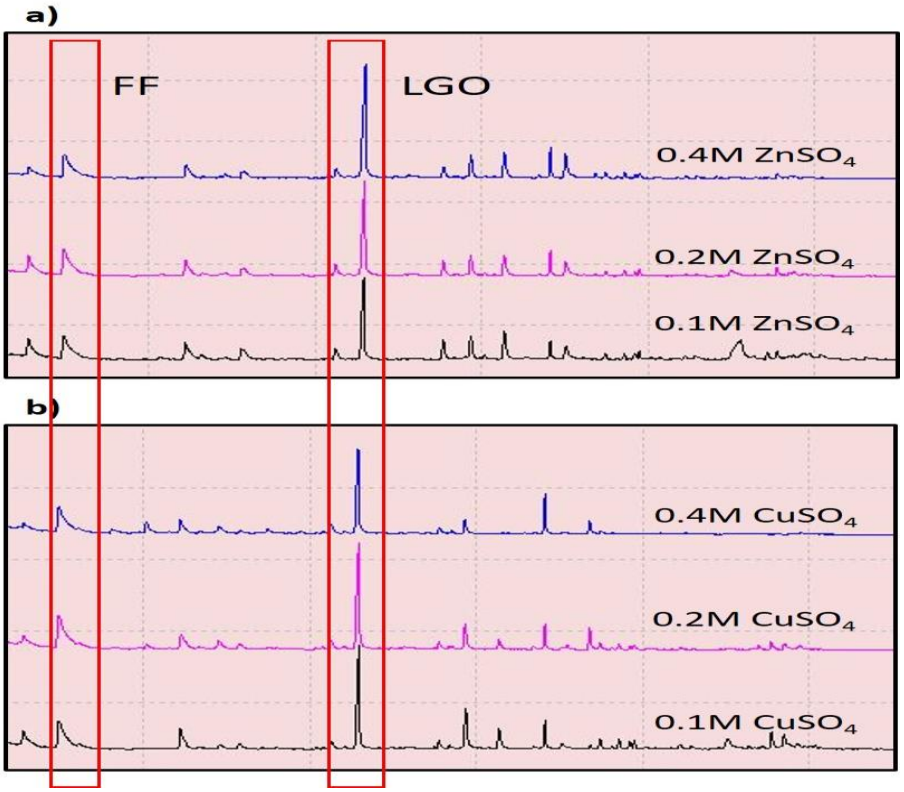

Figure 18. Ion chromatograms of Fraction 2 with a) $ZnSO_4$ and b) $CuSO_4$ at different concentrations

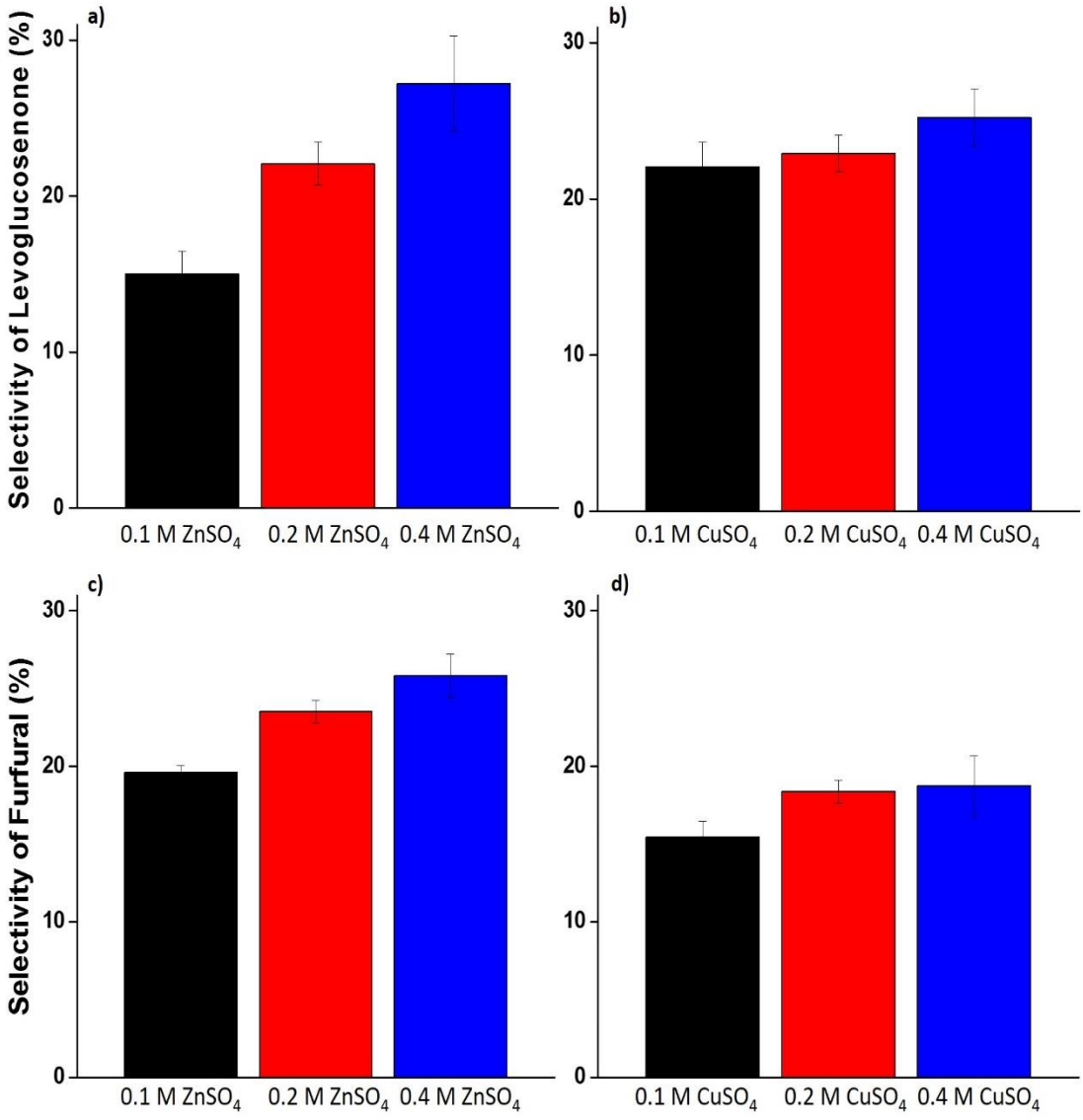

Figure 19. Selectivity of LGO for a) $ZnSO_4$ and b) $CuSO_4$ and selectivity of FF for c) $ZnSO_4$ and d) $CuSO_4$

4.3.6 Microwave treatment effects on the characteristics of Ashe Juniper waste

Table 15 shows the elemental composition of raw and microwave-treated Ashe Juniper waste. Carbon content decreased and oxygen content increased with microwave treatment compared to untreated Ashe juniper waste. This result is probably due to the removal of lignin content, which has the highest carbon and lowest oxygen content[82]. Ashe juniper waste treated with organic solvent including sulfuric acid exhibited the lowest carbon and highest oxygen content. Thus, it is confirmed that the sulfuric acid had a catalytic effect on composition change of Ashe juniper waste. Microwave treatment also increased O/C and H/C ratios of Ashe juniper waste; the highest O/C and H/C ratio were observed in for samples treated with solvents including sulfuric acid.

Thermogravimetric (TG) and differential thermogravimetric (DTG) analyses were performed for the characterization of pyrolysis characteristics of raw Ashe juniper and microwave-treated Ashe juniper waste, as shown in Figure 20. DTG curves show that microwave treatment shifted the peak of main decomposition stages to higher temperature. This observation is probably attributed to partial removal of lignin and extractable ash[82], which catalyze the pyrolysis reaction, by the microwave treatment. It is known that the decomposition temperatures[97] for hemicellulose, cellulose, and lignin are 220°C to 315°C, 315°C to 400°C, and 160°C to 900°C, respectively. Microwave-treated samples also exhibited a narrower range of decomposition temperature compared to raw Ashe juniper waste as shown in Figure 20a). Thus, this result means the microwave treatment changed the chemical composition of biomass waste. The yield of residue was increased after microwave-treatment as shown in Figure 20b). Acid promotes carbonization of sugar

released during pyrolysis[98], hence acid residues in treated samples may have facilitated carbonization of sugars during TG analysis.

Table 15. Elemental analysis and H/C, O/C, and S/C molar ratio

	Elemental analysis[a] *(wt %)*						
	C	H	N	O	S	H/C	O/C
A	48.6±0.4	6.66±0.07	0.11±0.01	44.6±0.4	0	1.62±0.00	0.69±0.02
B	47.6±0.2	6.43±0.03	0.10±0.01	45.8±0.2	0	1.64±0.01	0.72±0.01
C	46.5±0.3	6.38±0.02	0.11±0.00	47.0±0.3	0	1.65±0.01	0.76±0.01

A: Raw biomass, B: Microwave treated biomass without sulfuric acid, and C: Microwave treated biomass with sulfuric acid

4.3.7 Microwave treatment effects on product yields and selectivity of levoglucosan

Figure 15 shows product yields from vacuum pyrolysis of raw and microwave treated Ashe juniper waste samples. Microwave treatment did not significantly affect the yield of biochar. However, microwave treatment increased the yield of Fraction 2 and decreased the yield of Fraction 1. As shown in Figure 21, selectivity of levoglucosan increased from 5.9% to 53% after microwave treatment. Whereas, selectivity of phenolic compounds decreased from 20% to 5%. Since phenolic compounds are derived from lignin, this result suggests that microwave treatment partially removed lignin, which is consistent with elemental analysis result in section 4.3.5. It is expected that the

impregnation of either $ZnSO_4$ or $CuSO_4$ will improve selectivity of LGO due to the increased levoglucosan after microwave treatment.

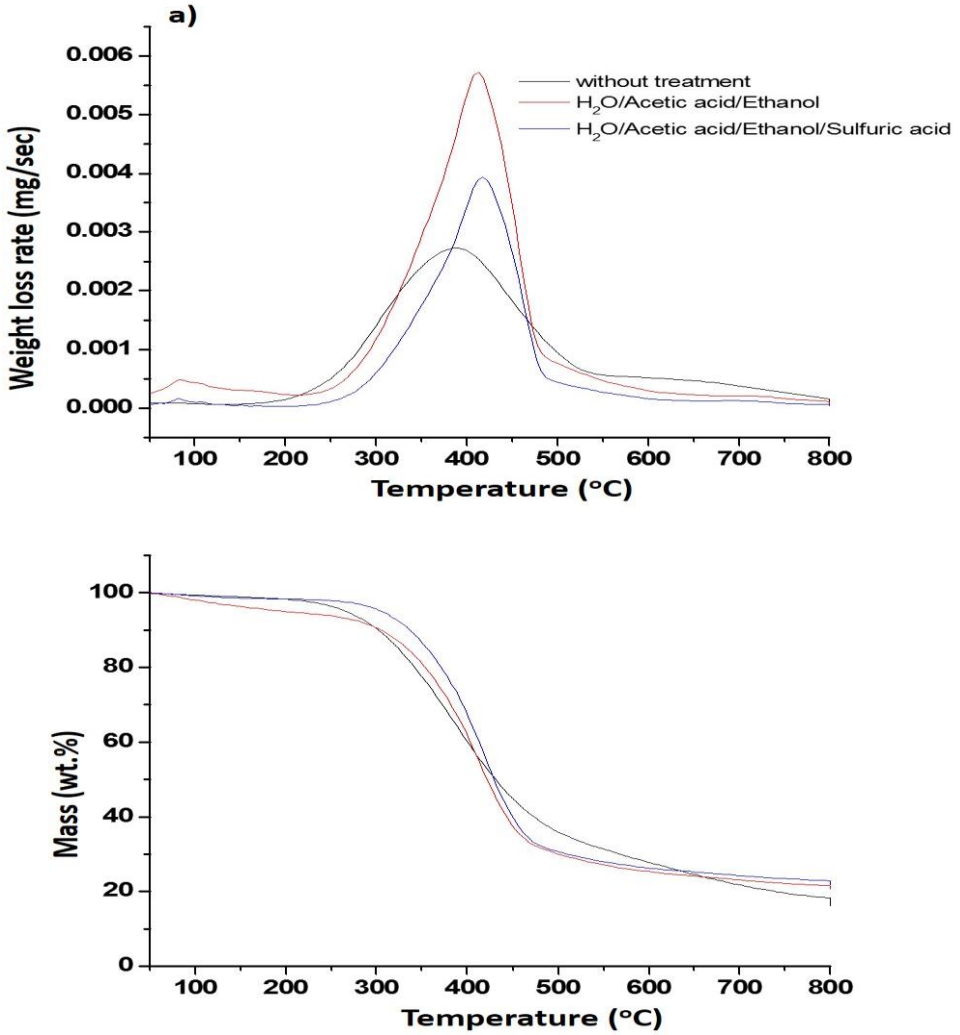

Figure 20. a) DTG of raw biomass and microwave treated biomass, and b) TGA of raw biomass and microwave treated biomass

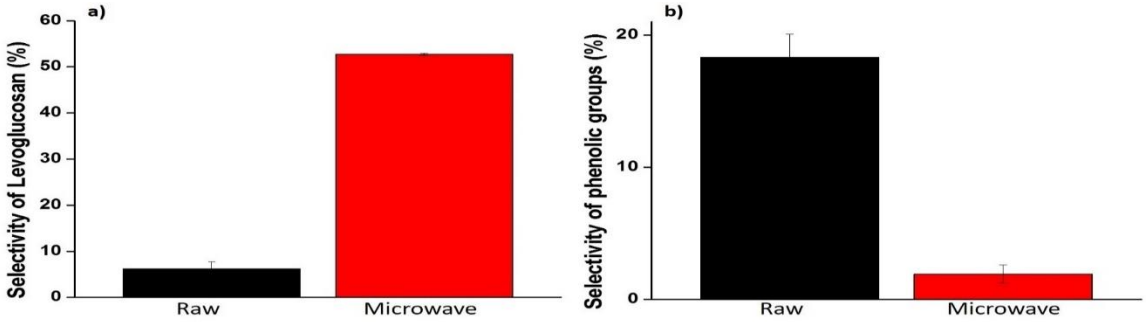

Figure 21. a) Selectivity of Levoglucosan and b) phenolic groups for raw biomass and microwave treated biomass

4.3.8 Economic analysis

Table 16 shows assumed parameters for economic analysis of LGO production. Vacuum pyrolysis plant[99] with the capacity of 94.5 dry MT of biomass per day was selected for the production of LGO. Current maximum yield of Levoglucosan from cellulose is 60%[82]. We assumed that whole levoglucosan is converted to LGO with the maximum yield of 78% based on stoichiometry. Therefore, the yield of LGO from biomass waste is about 19%. The initial investment capital was determined to be $40,552,646. The total fixed cost was obtained as $5,371,588 and total variable costs as $14,828,952. Currently, the price of Levoglucosan and LGO are $81.6/g and $125/g by Sigma Aldrich Co. LLC. However, the break-even cost of LGO in our assumed production process was $889/MT. The sensitivity analysis based on the selling price of LGO ranging from $889/MT to $1,020/MT was performed. At $1,020/MT, LGO production can make a net profit of $5,176,880 after the initial investment capital was paid off. PBP (payback

period) ranged from 19.41 to 6.26 years. IRR (internal return rate) increased from 0.1 to 15.2%, while, ROI (return of investment) increased from 5 to 16%.

Table 16. Assumed parameters for economic analysis

Parameter	Value
Feedstock throughput[100]	500 dry MT/day
Feedstock Cost[100]	$44.46/dry MT
Total vacuum pyrolysis plant installed cost[99]	$6,710,000/94.5 dry MT/day
Capacity[99]	94.5 dry MT/day
Pretreatment[101]	$5,050,000
Cellulose yield[50]	40 wt% (g/g biomass)
Levoglucosan yield[82]	60 wt% (g/g cellulose)
Levoglucosenone yield	78 wt% (g/g Levoglucosan)
Cost of Levoglucosenone	$889 to 1,020/MT
Operation life	20 years
Plant operation time	300 days/year
Interest	10%
Tax and insurance[101]	1.5% of total installed cost
Maintenance[101]	2% of equipment
Transportation of feedstock[100]	34% of feedstock total cost
Number of Manager	1
Salary of Manager	$50,000/year
Number and salary of operator	5 and $15/hr

4.4 Conclusions

Metal salt impregnation modified yield of products, chemical composition of bio-oil and selectivity of target chemicals. Metal sulfate impregnation was the way to produce LGO which is not produced from raw Ashe juniper waste and NaCl impregnated Ashe juniper waste. Metal sulfate concentrations had positive effects on the selectivity of LGO and FF. However, the cation played a different effect on the selectivity of LGO and FF; $ZnSO_4$ had more significant effect than $CuSO_4$. Biochar produced from metal-impregnated biomass has potential as functional biochar for adsorbents and catalysts. Microwave solvothermal treatment enhanced the selectivity of the levoglucosan from Ashe juniper waste. The combination of metal salt impregnation and microwave treatment is a promising method to achieve the optimum selectivity of LGO. The results of economic analysis of LGO production from the vacuum pyrolysis plant shows that PBP, IRR and ROI ranged from 6.26 to 19.41 years, 0.1 to 15.2% and 5 to 16% depending on the selling price of LGO

CHAPTER V

CONCLUSIONS AND FUTURE DIRECTION

In this dissertation, we successfully developed the method to tune the physicochemical properties of biochar using vacuum pyrolysis, functionalize the biochar to an adsorbent with high adsorption capacity and separation properties in the mixture, produce high value-added chemicals with the improved selectivity.

The method to control the properties of biochar was developed by the investigation of temperature and vacuum pressure which are process parameter of vacuum pyrolysis. By precise controlling of both parameters, elemental composition, the degree of carbonization, surface functionality, proximate analysis, and textile properties of biochar were significantly tailored. Specifically, the method enabled us to develop biochar having a higher degree of carbonization and well developed microporous structures (high surface area) compared to reported biochar. The application of vacuum pressure resulted in the production of biochar with lower H/C ratio and well developed-microporous structure at a lower temperature, which is a valuable improvement over biochar reported in the literature. By controlling the vacuum pressure and temperature, we could develop the biochar samples for several potential applications: B-520-3 as a carbon sequestration agent and B-450-1, 2, and 3 as good catalyst support and adsorbents for removal of MB. However, the method is only applied to Ashe juniper waste. Different type of biomass waste must be applied to generalize this method. Biochar is a promising soil amendment attracting many researchers. Furthermore, the properties as soil amendments such as

cationic exchange capacity, pH, and organic carbon should be investigated to confirm the influence of the method.

Sulfuric acid treatment produced surface functionalized biochar having high adsorption capacity on MB. The concentration of sulfuric acid is a key factor to control the adsorption capacity and physicochemical properties by introducing surface functional groups and microporosity. The adsorption capacity of MB on newly developed biochar increased 200-fold compared to raw biochar. The Langmuir isotherm was fit the data well indicating homogeneous surface, and the adsorption kinetics of MB on the sample followed Nth order kinetics. The binary system adsorption experiment revealed that the functionalized biochar with high adsorption capacity and selectivity on MB is a potential separator of MB from the dye mixtures produced from textiles and dyeing industry. To make biochar having improved properties, we need to investigate the effect of different oxidation reagents such as H_2O_2, HNO_3, and Acetic acid. There are several acid-treatment methods: evaporation, wet-impregnation, and fuming, etc. which should be tested. Also, the effect of the different pyrolysis technique such as conventional pyrolysis and vacuum pyrolysis on the degree of functionalization of biochar should be investigated. Finally, reaction time should be reduced, which is 24 hours currently, to improve economics. Biochar is a microwave absorbent. Rapid heating of biochar itself by absorption of the microwave will be a method to reduce reaction time. We should do regeneration test to evaluate economics of biochar-based adsorption process.

Metal salt impregnation and microwave solvothermal treatment modified yield of products, chemical composition of bio-oil and selectivity of target chemicals. LGO was

not produced from raw Ashe Juniper. However, metal sulfate impregnation produced LGO by dehydration of levoglucosan. Also, metal impregnation improved the selectivity of FF. The concentration of $ZnSO_4$ and $CuSO_4$ had positive effects on the selectivity of LGO and FF, while, $ZnSO_4$ had a more significant effect than $CuSO_4$. Microwave solvothermal treatment enhanced the selectivity of the levoglucosan by ten times. Therefore, the synergistic effect of metal sulfates impregnation and microwave solvothermal treatment for the optimum selectivity of LGO is expected. In the future, we need to investigate the effect of both methods on the yield of LGO, FF, and levoglucosan. Especially, different impregnation method should be tested to minimize the number of catalysts. Different organic solvents and process parameter should be investigated to develop the efficient method to alter the chemical composition of biomass for microwave pretreatment. Biochar produced from metal-impregnated biomass contains metal salts. We should recover these metal salts and do regeneration test on catalytic pyrolysis. We should obtain yields of products and conversion of biomass using GC-FID, for the yield of acids, and HPLC for the yield of Levoglucosenone. To increase the yield of target chemicals, we should test organic solvent based extraction method. To purify the target chemicals, advanced purification method such as supercritical fluid extraction and molecular distillation should be developed and tested. Finally, we should do thecno-economic evaluation to compare this process to currently developed process.

REFERENCES

1. H. An, W. E. Wilhelm and S. W. Searcy, Biomass and Bioenergy **35** (9), 3763-3774 (2011).
2. G. Kabir and B. H. Hameed, Renewable and Sustainable Energy Reviews **70**, 945-967 (2017).
3. R. A. Sheldon, Green Chemistry **16** (3), 950-963 (2014).
4. J. K. Saini, R. Saini and L. Tewari, 3 Biotech **5** (4), 337-353 (2015).
5. M. Arshadi, T. M. Attard, R. M. Lukasik, M. Brncic, A. M. da Costa Lopes, M. Finell, P. Geladi, L. N. Gerschenson, F. Gogus, M. Herrero, A. J. Hunt, E. Ibanez, B. Kamm, I. Mateos-Aparicio, A. Matias, N. E. Mavroudis, E. Montoneri, A. R. C. Morais, C. Nilsson, E. H. Papaioannou, A. Richel, P. Ruperez, B. Skrbic, M. Bodroza Solarov, J. Svarc-Gajic, K. W. Waldron and F. J. Yuste-Cordoba, Green Chemistry **18** (23), 6160-6204 (2016).
6. D. Carpenter, T. L. Westover, S. Czernik and W. Jablonski, Green Chemistry **16** (2), 384-406 (2014).
7. H. Kovacs and K. Szemmelveisz, Chemosphere **166**, 8-20 (2017).
8. W.-J. Liu, H. Jiang and H.-Q. Yu, Chemical Reviews **115** (22), 12251-12285 (2015).
9. K. Qian, A. Kumar, H. Zhang, D. Bellmer and R. Huhnke, Renewable and Sustainable Energy Reviews **42**, 1055-1064 (2015).

10. D. Czajczyńska, L. Anguilano, H. Ghazal, R. Krzyżyńska, A. J. Reynolds, N. Spencer and H. Jouhara, Thermal Science and Engineering Progress **3**, 171-197 (2017).

11. J. J. Manyà, Environmental Science & Technology **46** (15), 7939-7954 (2012).

12. S. P. Sohi, E. Krull, E. Lopez-Capel and R. Bol, in *Advances in Agronomy* **105**, 47-82 (2010).

13. A. Anca-Couce, Progress in Energy and Combustion Science **53**, 41-79 (2016).

14. L. Zhao, X. Cao, O. Mašek and A. Zimmerman, Journal of Hazardous Materials **256–257**, 1-9 (2013).

15. J. J. Manyà, S. Laguarta, M. A. Ortigosa and J. A. Manso, Energy & Fuels **28** (5), 3271-3280 (2014).

16. M. Azuara, B. Baguer, J. I. Villacampa, N. Hedin and J. J. Manyà, Fuel **186**, 525-533 (2016).

17. D. Mohan, A. Sarswat, Y. S. Ok and C. U. Pittman Jr, Bioresource Technology **160**, 191-202 (2014).

18. X. Xiao, Z. Chen and B. Chen, Scientific Reports **6**, 22644 (2016).

19. R. Azargohar, S. Nanda, J. A. Kozinski, A. K. Dalai and R. Sutarto, Fuel **125**, 90-100 (2014).

20. M. I. Al-Wabel, A. Al-Omran, A. H. El-Naggar, M. Nadeem and A. R. A. Usman, Bioresource Technology **131**, 374-379 (2013).

21. L. Wang, Ø. Skreiberg, M. Gronli, G. P. Specht and M. J. Antal, Energy & Fuels **27** (4), 2146-2156 (2013).

22. S. Van Wesenbeeck, C. Higashi, M. Legarra, L. Wang and M. J. Antal, Energy & Fuels **30** (1), 480-491 (2016).

23. E. Cetin, B. Moghtaderi, R. Gupta and T. F. Wall, Fuel **83** (16), 2139-2150 (2004).

24. F. Melligan, R. Auccaise, E. H. Novotny, J. J. Leahy, M. H. B. Hayes and W. Kwapinski, Bioresource Technology **102** (3), 3466-3470 (2011).

25. A. U. Rajapaksha, S. S. Chen, D. C. W. Tsang, M. Zhang, M. Vithanage, S. Mandal, B. Gao, N. S. Bolan and Y. S. Ok, Chemosphere **148**, 276-291 (2016).

26. K. A. Thompson, K. K. Shimabuku, J. P. Kearns, D. R. U. Knappe, R. S. Summers and S. M. Cook, Environmental Science & Technology **50** (20), 11253-11262 (2016).

27. G. Ding, B. Wang, L. Chen and S. Zhao, Chemosphere **163**, 283-289 (2016).

28. X. Meng, H. Zhang, C. Liu and R. Xiao, Energy & Fuels **30** (10), 8369-8376 (2016).

29. F. Cao, T. J. Schwartz, D. J. McClelland, S. H. Krishna, J. A. Dumesic and G. W. Huber, Energy & Environmental Science **8** (6), 1808-1815 (2015).

30. M. De bruyn, J. Fan, V. L. Budarin, D. J. Macquarrie, L. D. Gomez, R. Simister, T. J. Farmer, W. D. Raverty, S. J. McQueen-Mason and J. H. Clark, Energy & Environmental Science **9** (8), 2571-2574 (2016).

31. S. Wang, Biomass Now - Sustainable Growth and Use, Chapter 16 (2013).

32. G. Dobele, T. Dizhbite, G. Rossinskaja, G. Telysheva, D. Meier, S. Radtke and O. Faix, Journal of Analytical and Applied Pyrolysis **68–69**, 197-211 (2003).

33. G. Dobele, G. Rossinskaja, G. Telysheva, D. Meier and O. Faix, Journal of Analytical and Applied Pyrolysis **49** (1–2), 307-317 (1999).

34. G. Dobele, G. Rossinskaja, T. Dizhbite, G. Telysheva, D. Meier and O. Faix, Journal of Analytical and Applied Pyrolysis **74** (1–2), 401-405 (2005).

35. C. Branca, A. Galgano, C. Blasi, M. Esposito and C. Di Blasi, Energy & Fuels **25** (1), 359-369 (2011).

36. X. Wei, Z. Wang, Y. Wu, Z. Yu, J. Jin and K. Wu, Journal of Analytical and Applied Pyrolysis **107**, 150-154 (2014).

37. Q. Lu, X.-n. Ye, Z.-b. Zhang, C.-q. Dong and Y. Zhang, Bioresource Technology **171**, 10-15 (2014).

38. A. McGinty, the Brush Sculptors: Innovations for tailoring brushy rangelands to enhance wildlife habitat and recreational value, Proceedings of a Conference, (1997).

39. F. Smeins and S. Fuhlendorf, Texas Agricultural Experiment Station Technical Report, San Angelo, TX, USA 1997.

40. R. K. Lyons, M. K. Owens and R. V. Machen, Juniper biology and management in Texas, (1998).

41. M. Garriga, A. Thurow, T. Thurow, R. Conner, D. Brandenberger and C. Taylor Jr, Texas Agricultural Experiment Station Technical Report, San Angelo, Texas, USA (1997).

42. M. W. Turner, Remarkable plants of Texas: uncommon accounts of our common natives, (2009).

43. M. Jahirul, M. Rasul, A. Chowdhury and N. Ashwath, Energies **5** (12), 4952 (2012).

44. T. M. Alslaibi, I. Abustan, M. A. Ahmad and A. A. Foul, Journal of Chemical Technology & Biotechnology **88** (7), 1183-1190 (2013).

45. M. Amutio, G. Lopez, R. Aguado, M. Artetxe, J. Bilbao and M. Olazar, Energy & Fuels **25** (9), 3950-3960 (2011).

46. Standard Practice for Proximate Analysis of Coal and Coke, in, ASTM International, (2013).

47. S. Brunauer, P. H. Emmett and E. Teller, Journal of the American Chemical Society **60** (2), 309-319 (1938).

48. M. M. Dubinin and H. F. Stoeckli, Journal of Colloid and Interface Science **75** (1), 34-42 (1980).

49. J. Park, Y. Lee, C. Ryu and Y.-K. Park, Bioresource Technology **155**, 63-70 (2014).

50. S. Capareda, Introduction to biomass energy conversions, (2013).

51. U. Moralı, N. Yavuzel and S. Şensöz, Bioresource Technology **221**, 682-685 (2016).

52. L. Wang, M. Trninic, Ø. Skreiberg, M. Gronli, R. Considine and M. J. Antal, Energy & Fuels **25** (7), 3251-3265 (2011).

53. C. Di Blasi, Progress in Energy and Combustion Science **34** (1), 47-90 (2008).

54. S. Yi, B. Gao, Y. Sun, J. Wu, X. Shi, B. Wu and X. Hu, Chemosphere **150**, 694-701 (2016).

55. M. Qiu, K. Sun, J. Jin, B. Gao, Y. Yan, L. Han, F. Wu and B. Xing, Scientific Reports **4**, 5295 (2014).

56. M. Keiluweit, P. S. Nico, M. G. Johnson and M. Kleber, Environmental Science & Technology **44** (4), 1247-1253 (2010).

57. K. H. Kim, J.-Y. Kim, T.-S. Cho and J. W. Choi, Bioresource Technology **118**, 158-162 (2012).

58. J. A. Ippolito, D. A. Laird and W. J. Busscher, Journal of Environmental Quality **41** (4), 967-972 (2012).

59. P. Liu, W.-J. Liu, H. Jiang, J.-J. Chen, W.-W. Li and H.-Q. Yu, Bioresource Technology **121**, 235-240 (2012).

60. S. Kloss, F. Zehetner, A. Dellantonio, R. Hamid, F. Ottner, V. Liedtke, M. Schwanninger, M. H. Gerzabek and G. Soja, Journal of Environmental Quality **41** (4), 990-1000 (2012).

61. L. Luo, C. Xu, Z. Chen and S. Zhang, Bioresource Technology **192**, 83-89 (2015).

62. F. N. D. Mukome, X. Zhang, L. C. R. Silva, J. Six and S. J. Parikh, Journal of Agricultural and Food Chemistry **61** (9), 2196-2204 (2013).

63. S. Prapagdee, S. Piyatiratitivorakul and A. Petsom, EnvironmentAsia **7** (2), 60-69 (2014).

64. T. M. Suguihiro, P. R. de Oliveira, E. I. P. de Rezende, A. S. Mangrich, L. H. Marcolino Junior and M. F. Bergamini, Bioresource Technology **143**, 40-45 (2013).

65. K. Komnitsas, D. Zaharaki, I. Pyliotis, D. Vamvuka and G. Bartzas, Waste and Biomass Valorization **6** (5), 805-816 (2015).

66. S. Ismadji, Y. Sudaryanto, S. B. Hartono, L. E. K. Setiawan and A. Ayucitra, Bioresource Technology **96** (12), 1364-1369 (2005).

67. J. Yang and K. Qiu, Chemical Engineering Journal **165** (1), 209-217 (2010).

68. G. Yang, L. Wu, Q. Xian, F. Shen, J. Wu and Y. Zhang, PLOS ONE **11** (5), (2016).

69. R. Gong, J. Ye, W. Dai, X. Yan, J. Hu, X. Hu, S. Li and H. Huang, Industrial & Engineering Chemistry Research **52** (39), 14297-14303 (2013).

70. Y. Han, A. A. Boateng, P. X. Qi, I. M. Lima and J. Chang, Journal of Environmental Management **118**, 196-204 (2013).

71. I. Ali, Chemical Reviews **112** (10), 5073-5091 (2012).

72. P. Wang, C. Wu, Y. Guo and C. Wang, Physical Chemistry Chemical Physics **18** (43), 30196-30203 (2016).

73. K. Y. Foo and B. H. Hameed, Chemical Engineering Journal **156** (1), 2-10 (2010).

74. R. Xing, Y. Liu, Y. Wang, L. Chen, H. Wu, Y. Jiang, M. He and P. Wu, Microporous and Mesoporous Materials **105** (1), 41-48 (2007).

75. J.-Y. Lai, Y.-T. Li and T.-P. Wang, International Journal of Molecular Sciences **11** (12), 5256-5272 (2010).

76. F. Güzel, H. Sayğılı, G. Akkaya Sayğılı, F. Koyuncu and C. Yılmaz, Journal of Cleaner Production **144**, 260-265 (2017).

77. H. M. Abd El Salam, S. A. Younis, H. R. Ali and T. Zaki, Microporous and Mesoporous Materials **241**, 210-217 (2017).

78. M. Arulkumar, P. Sathishkumar and T. Palvannan, Journal of Hazardous Materials **186** (1), 827-834 (2011).

79. M. S. S, E. A. A. M and R. Chidambaram, PLOS ONE **10** (3), (2015).

80. D. D. Sewu, P. Boakye and S. H. Woo, Bioresource Technology **224**, 206-213 (2017).

81. H. Cherifi, B. Fatiha and H. Salah, Applied Surface Science **282**, 52-59 (2013).

82. A. Zheng, Z. Zhao, Z. Huang, K. Zhao, G. Wei, L. Jiang, X. Wang, F. He and H. Li, Green Chemistry **17** (2), 1167-1175 (2015).

83. B. Zhang, E. Leng, P. Wang, X. Gong, J. Zhang, Y. Zhang and M. Xu, Journal of Analytical and Applied Pyrolysis **114**, 119-126 (2015).

84. X. Cao, S. P. Teong, D. Wu, G. Yi, H. Su and Y. Zhang, Green Chemistry **17** (4), 2348-2352 (2015).

85. Y. Long, Y. Yu, Y. W. Chua and H. Wu, Fuel **193**, 460-466 (2017).

86. A. K. Kumar and S. Sharma, Bioresources and Bioprocessing **4** (1), 7 (2017).

87. H. Li, Y. Qu, Y. Yang, S. Chang and J. Xu, Bioresource Technology **199**, 34-41 (2016).

88. H. M. Mohd, American Journal of Applied Sciences **8** (11), 1135 (2011).

89. G. A. Burdock, Encyclopedia of food and color additives, (1997).

90. J. N. Chheda, Y. Roman-Leshkov and J. A. Dumesic, Green Chemistry **9** (4), 342-350 (2007).

91. R. Dubey, S. Jakeer and N. A. Gaur, Journal of Bioscience and Bioengineering **121** (5), 509-516 (2016).

92. W. Steglich, B. Fugmann and S. Lang-Fugmann, ROMPP Encyclopedia Natural Products, (2000).

93. P. Rutkowski, Journal of Analytical and Applied Pyrolysis **98**, 86-97 (2012).

94. S. Xing, H. Yuan, Huhetaoli, Y. Qi, P. Lv, Z. Yuan and Y. Chen, Energy **114**, 634-646 (2016).

95. P. R. Patwardhan, J. A. Satrio, R. C. Brown and B. H. Shanks, Bioresource Technology **101** (12), 4646-4655 (2010).

96. H. Zhang, X. Liu, M. Lu, X. Hu, L. Lu, X. Tian and J. Ji, Bioresource Technology **169**, 800-803 (2014).

97. C. Liu, H. Wang, A. M. Karim, J. Sun and Y. Wang, Chemical Society Reviews **43** (22), 7594-7623 (2014).

98. D. L. Dalluge, T. Daugaard, P. Johnston, N. Kuzhiyil, M. M. Wright and R. C. Brown, Green Chemistry **16** (9), 4144-4155 (2014).

99. A. V. Bridgwater, Advances in thermochemical biomass conversion, (2013).

100. J. J. Juárez, V. R. Contreras, G. R. Haupert, S. Hill and D. E. Daugaard, Proceedings of PWR2006, 585-590 (2006).

101. M. Ringer, V. Putsche and J. Scahill, Large-scale pyrolysis oil production:a technology assessment and economic analysis, (2006).